Reaction mechanisms of the O2 reduction/evolution reaction

Gattrell, M.; MacDougall, B.

Handbook of Fuel Cells: Fundamentals, Technology and Applications, Electrocatalysis 2, pp. 443-464, 2003-01-01

Chapter 30

Reaction mechanisms of the O_2 reduction/evolution reaction

M. Gattrell and B. MacDougall

Institute for Chemical Process and Environmental Technology, Ottawa, Canada

1 INTRODUCTION

The electrochemistry of oxygen (its reduction to water and evolution from water) has been extensively and intensively studied because of its fundamental complexity and importance for many practical systems. Oxygen reduction is the key to achieving the overall fuel oxidation reaction in fuel cells. It is also of interest for metal–air batteries, and as a cathodic reaction to reduce the cell voltage in electrochemical processes. A deep understanding of oxygen reduction is also important because it is often the counter electrode reaction for many corrosion systems. Oxygen evolution occurs in electrolyzers, as a counter electrode reaction for electrowinning, and as a competing process for many oxidative synthesis reactions (e.g., chlorine, ozone). It is also important for recharging of metal–air batteries and regenerative fuel cells. One interesting application combining both reactions is electrochemical oxygen pumps. These reduce oxygen at one electrode from a low pressure and/or low purity feed stream, then evolve oxygen from the other electrode at high purity and possibly also high pressure.

The reaction is also of fundamental interest because it is a good example of an electrocatalytic reaction (thus involving adsorption) and so shows a great sensitivity to the electrode surface and the presence of other adsorbed species. Studies have been carried out investigating the effects of different electrode materials, different crystal faces, surface modification by adatoms, and the influence of different electrolytes or contaminants.

The progress made in the understanding of oxygen electrochemistry over the years and by different groups has been the subject of numerous reviews. These include those by J. P. Hoare (1968),[1] A. Damjanovic (1969),[2] J. P. Hoare (1974),[3] M. R. Tarasevich, A. Sadkowski, and E. Yeager (1983),[4] A. J. Appleby (1992),[5] A. Damjanovic (1992),[6] K. Kinoshita (1992),[7] J. O'M. Bockris (1993),[8] R. Adzic (1998),[9] among others.

The importance of better understanding, and so hopefully better catalyzing, the oxygen reduction reaction can be seen in the high overvoltage in an operating fuel cell related to oxygen reduction (see Figure 1). Being from a real fuel cell, these curves also reflect some transport limits within the catalyst and backing layers in addition to the kinetic losses. However, for the 5 atm results, where the transport losses have been estimated to be small, the electrode potential is still about 400 mV below the theoretical potential. The potential drop at the cathode is even more important for direct methanol fuel cells, where methanol that crosses the cell membrane further decreases the cathode potential.

The overall reaction for the 4-electron reduction of oxygen to water is shown below

$$\text{(In acid) } O_2 + 4e^- + 4H^+ \longrightarrow 2H_2O$$
$$E_0 = 1.229\,\text{V vs. SHE} \qquad (1)$$

From thermodynamic data, the potential has been calculated to be 1.229 V vs. standard hydrogen electrode (SHE).[4] The reaction, however, involves multiple intermediates,

Handbook of Fuel Cells – Fundamentals, Technology and Applications, Edited by Wolf Vielstich, Hubert A. Gasteiger, Arnold Lamm. Volume 2: *Electrocatalysis*. ISBN: 0-471-49926-9.

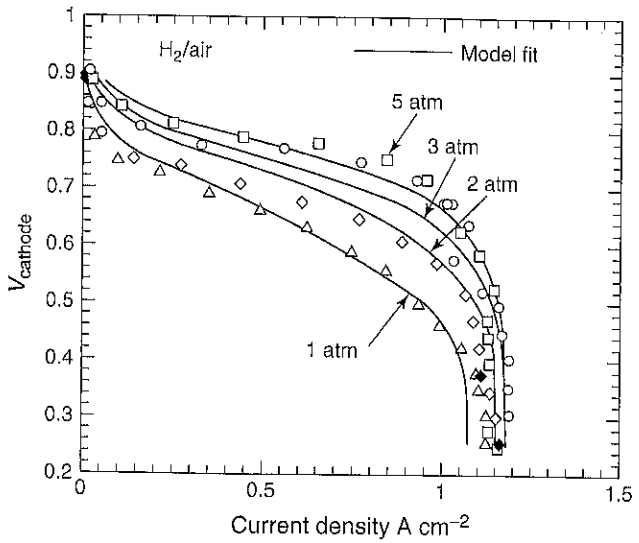

Figure 1. Cathode polarization curves for an H_2/air solid polymer electrolyte (SPE) fuel cell. (Voltage vs. RHE, ohmic drop (IR) corrected, 25 cm^2 membrane area, 5 μm catalyst layer thickness, limiting current due to flooding). The theoretical potential would be 1.229 V for 1 atm of oxygen. (Reproduced from Springer *et al.* (1993)[10] by permission of The Electrochemical Society.)

electron transfers, and reaction steps. A diagram of the various possible intermediates and their chemical potentials in acidic water is shown in Figure 2.[11] It can be imagined from the diagram that many different routes can operate. The real situation is far more complicated because the various intermediates will most likely interact with an electrode surface and so their chemical potential will depend on the local environment. This includes the nature of the electrode surface at the site of the intermediate's adsorption, as well as the influence of neighboring adsorbates and the electrolyte. Also, such a diagram does not show the activation energies required to move from one intermediate to another.

In some of the literature, a distinction has been made between the *parallel* path involving dissociation of the oxygen and its subsequent reduction to water, and the *series* path involving the formation of hydrogen peroxide, which can be a final product or an intermediate leading also to water. From Figure 2, it can be seen that a parallel path involving an atomic oxygen type intermediate would require an electrode surface that could significantly reduce the chemical potential of the intermediate. In fact, such a pathway has only been suggested for a few metals including Pt, Pd, Ag, and the 100 face of Au. Most other materials, including different carbons, Hg, Au (other than the 100 face), and oxide covered metals, tend to follow a 2-electron reduction path leading to a peroxide product. (It should be noted that transition metal macrocycle catalysts, and oxygen reduction at metal oxides at high temperatures (where

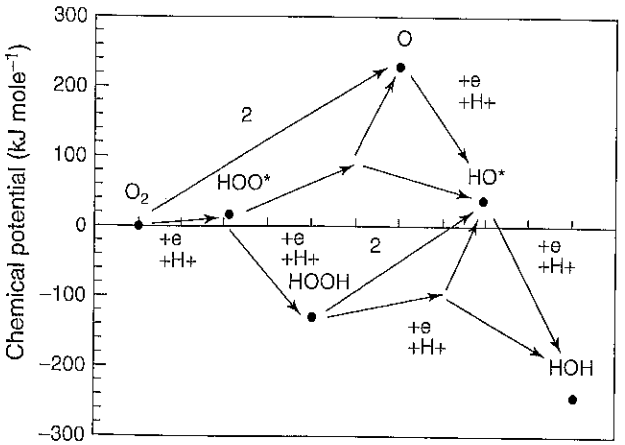

Figure 2. The chemical potentials of various oxygen reduction intermediates in acidic water. (Note the pk_a of H_2O_2 is 11.6 and of HO_2 is 7.3). (Data from Ref. [11].)

O^{2-} is the final product), is dealt with in **Macrocycles**, Volume 2 and **O_2-reduction at high temperatures: SOFC**, Volume 2.) The 2-electron oxygen reduction reaction is shown below

$$\text{(In acid) } O_2 + 2e^- + 2H^+ \longrightarrow H_2O_2$$
$$E_0 = 0.67\text{ V vs. SHE} \qquad (2)$$

The peroxide produced can be further reduced (leading to a series path 4-electron reduction)

$$\text{(In acid) } H_2O_2 + 2e^- + 2H^+ \longrightarrow 2H_2O$$
$$E_0 = 1.77\text{ V vs. SHE} \qquad (3)$$

or it can decompose either homogeneously or heterogeneously (also yielding an overall 4-electron reduction)

$$2H_2O_2 \longrightarrow O_2 + 2H_2O \qquad (4)$$

In fuel cells, in order to obtain maximum efficiency and to avoid corrosion of carbon supports and other materials by peroxide, it is desired to achieve a 4-electron reduction.[12] The 2-electron reduction is of practical interest for the production of hydrogen peroxide.[13]

Pt or Pt-based catalysts are still the most important catalysts for oxygen reduction for fuel cells and so the mechanisms of oxygen reduction at Pt will be the first focus of this chapter.

2 OXYGEN REDUCTION ON PLATINUM

Oxygen reduction at platinum is characterized under most conditions by a 4-electron reaction. Under typical

conditions, the oxygen reduction intermediate species share the electrode surface with platinum oxide and/or hydroxide compounds as well as other adsorbed species. The formation of platinum oxide and/or hydroxide compounds shows an irreversible behavior and so the performance of a platinum electrode may also depend on its history. The sensitivity of the reaction to other adsorbed species has also meant that great care has had to be taken to avoid trace impurities during measurements.

2.1 Platinum surface characteristics

It is important in understanding oxygen reduction to understand the state of the platinum surface. The key platinum surface states are nicely illustrated by the series of voltammograms shown in Figure 3. The reversible adsorption/desorption of hydrogen can be seen below about 0.3 V. Over short time spans, the adsorption of OH behaves reversibly from about 0.8 V up to almost 1.0 V, beyond which irreversible adsorption occurs. The irreversibly adsorbed oxygen is gradually reduced beginning at potentials of about 0.95 V and becoming progressively faster at lower potentials. This irreversibility is generally felt to be due to a transformation of the adsorbed layer into a surface phase oxide by a place exchange mechanism. It is also interesting that, in spite of the irreversible transformation of the adsorbed species, further adsorption up to 1.4 V appears to follow the characteristic current–voltage profile typical of a Temkin type isotherm. Thus, while no true reversible isotherm exists involving the surface oxide species, there appears to be interactions between the freshly adsorbing OH and the place exchanged oxygen species. This is not to imply, however, that the oxygen species coverages are only potential dependent as changes in the film stability have been noted when anodes were held at constant potentials above 0.9 V, and film thickening noted at potentials above 1.4 V.[14] (It should be noted that these potentials are for polycrystalline platinum electrodes. Different potential regions have been noted for single crystal platinum and for platinum nanoparticles (these areas will be discussed in more detail in the following chapters)).

The influence of surface oxides on the oxygen reduction reaction can be clearly seen in Figure 4 where polarization curves for oxygen at pre-reduced and pre-oxidized platinum electrodes are shown. There is a clear difference in the Tafel slopes, which change from $-120\,\text{mV decade}^{-1}$ for the pre-oxidized electrode to $-60\,\text{mV decade}^{-1}$ for the pre-reduced electrode. (It should be noted that while the Tafel measurements at the pre-reduced electrode are true steady state values, those for the pre-oxidized electrodes were obtained fairly quickly to avoid oxide reduction.) It is also interesting that the plot for the pre-reduced platinum does not extend above 1.0 V, as this was the experimentally

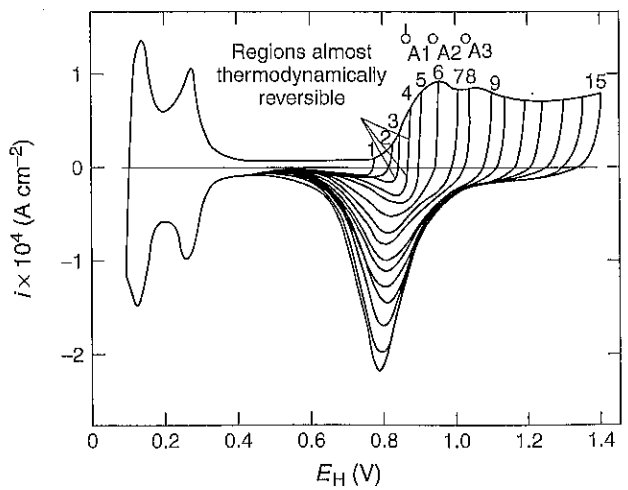

Figure 3. Platinum electrode voltammograms showing the reversible and irreversible regimes for the formation of platinum oxide species. (0.5 M H_2SO_4, 100 mV s^{-1}, E_H = RHE). (Reproduced from Angerstein-Kozlowska *et al.* (1973)[14] by permission of Elsevier Science.)

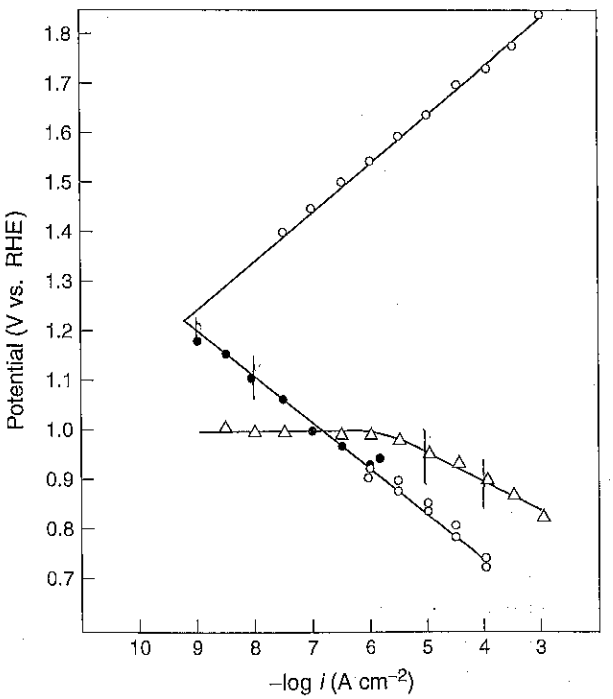

Figure 4. Cathodic and anodic Tafel lines for oxygen reduction on oxide covered and pre-reduced Pt electrodes in acidic solutions. • obtained by slow polarization of a pre-oxidized electrode starting from open circuit, ○ obtained by stepping an oxidized electrode to the desired current, Δ obtained at the pre-reduced electrode. (H.E. = RHE). (Reproduced from Damjanovic and Bockris (1966)[15] by permission of Elsevier Science.)

observed rest potential in the oxygen saturated solution (discussed below).

The platinum surface of an oxygen reduction catalyst in an operating fuel cell would be expected to correspond with the steady state results obtained with the pre-reduced platinum (i.e., it will be partially covered with adsorbed oxygen species). Therefore most research has focused on this type of platinum surface.

2.2 Open circuit potential and exchange current density

One difficulty for the study of the oxygen reduction reaction (as well as for practical applications) is its very low exchange current density (around 10^{-10} A cm^{-2} (see Figure 4)). This makes experimental measurement of the thermodynamic rest potential difficult because of the possible influence of other reactions. Indeed, even with carefully prepared systems, the rest potential measured at a platinum electrode with 1 atm of oxygen rarely exceeds 1.1 V vs. normal hydrogen electrode (NHE).[4] The typical open circuit potential for oxygen electrodes in fuels cells is around 1.0 V vs. NHE. (In Figure 4 the rest potential is about 1.0 V with an apparent exchange current density of about 10^{-7}–10^{-6} A cm^{-2}). Successful equilibrium potential measurements have been made only in high purity solutions and after extensive pre-oxidation of the platinum electrode. Even then the potential was often only stable for a few hours. Such a cathodic shift in the open circuit potential from the thermodynamic potential would need to be powered by some anodic reaction (in the case of Figure 4 this reaction would have to provide a current of about 10^{-7}–10^{-6} A cm^{-2} to balance the oxygen reduction current at that potential). Various possible reactions have been proposed (and are discussed in detail elsewhere)[4] including trace organic contaminant oxidation, oxide formation, or platinum corrosion, with the latter mechanism now considered to best fit the data. This platinum corrosion is reported to start at about 0.5 V vs. SHE in 2 M H_2SO_4 at about 10^{-9} A cm^{-2}, then increase to a mass transfer limited current of about 10^{-7}–10^{-6} A cm^{-2} at about 0.8–0.9 V vs. SHE. The characteristics of such a corrosion reaction appear to provide a reasonable explanation for the observed rest potentials at least in the acidic (pH 0–3) and basic (pH 11–14) regions, while contaminants may still play a role in the neutral regions.[16] This corrosion can, however, be greatly decreased after forming a phase oxide on the platinum surface, thus explaining the ability to successfully measure the thermodynamic open circuit potential at pre-oxidized electrodes.

2.3 Mechanism and kinetics

Oxygen reduction on platinum occurs predominately through a 4-electron oxidation to water (or to OH^- in base). The mechanism is complicated because of the various oxygen reduction intermediates, as well as platinum surface oxides and/or hydroxides. Experimentally measured oxygen reduction electrochemical parameters can provide information only up to the rate-determining step. Because of the slow kinetics of the reaction, the reverse reaction (oxygen evolution) occurs at a significantly higher potential where a phase oxide exists on the platinum surface. This change in the electrode surface means that the electrochemical characteristics of the reverse reaction cannot provide information on the reaction steps for oxygen reduction that follow the rate-determining step. Therefore, many different methods have been used to try to fully understand the mechanism and the results have sometimes been inconclusive.

2.3.1 Tafel slopes, reaction orders

A significant amount of experimental work has been done to measure the reaction orders and Tafel slopes for oxygen reduction on platinum. When trying to interpret the results, however, one must bear in mind that the state of the platinum surface can change with potential.

This area has been intensively studied by many people and has at times been the subject of some controversy. A key researcher has been Damjanovic, who started researching the area with Bockris in the 1960s, and continued until the early 1990s. In early work, it was noted that the Tafel slope and reaction orders were different depending on the potential region and pH of the measurements. In acidic solutions (of perchloric acid or sulfuric acid) one potential region was observed where partial coverage of oxide species existed (approx. 1.0–0.8 V vs. RHE). In this range, the Tafel slope was measured as -60 mV decade^{-1}, and the reaction orders were 1 with respect to oxygen pressure, and 1.67 with respect to pH (measured over a small range from pH 1 to 2.2).[17] The second region occurred at larger cathodic current densities that yielded potentials where the platinum was oxide free (from approx. 0.8 V to the onset of hydrogen adsorption at approx. 0.35 V vs. RHE). In this range, the Tafel slope was measured as -120 mV decade^{-1}, and the reaction orders were one with respect to oxygen pressure, and one with respect to pH.[17]

In the partial oxide coverage region, the results were explained by observing that the coverage by oxide species (PtOH or PtO) is essentially linear with potential and shifts with pH (see Figure 5). Hence, a Temkin isotherm for the

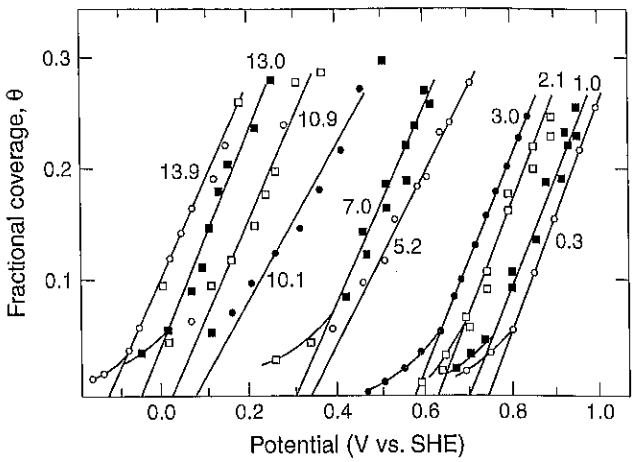

Figure 5. Dependence with potential of the coverage of a platinum electrode by oxygen-containing species, measured at various pH values. (Reproduced from Sepa *et al.* (1981)[20] by permission of Elsevier Science.)

adsorbed oxygen species might be assumed, given by

$$\theta = \frac{F}{\gamma}\left(E + \frac{2.3RT}{F}\text{pH} - E_0\right) \tag{5}$$

where γ is a constant and E_0 is the potential at the onset of adsorption of oxygen species on the platinum surface at pH = 0. It was then assumed that the surface oxygen intermediates produced by oxygen reduction interact equivalently with and/or are identical with the surface oxygen species produced on polarization of platinum in aqueous solutions. If so, the enthalpy of activation for a reaction step producing an adsorbed oxygen species will contain some fraction (given by a symmetry factor α) of the enthalpy of adsorption of the product. This will vary with the coverage of oxygen species on the electrode surface, which in turn is a function of potential and pH.

$$\Delta G^*_\theta = \Delta G^*_{E=E_0} + \alpha\gamma\theta \tag{6}$$

where $\Delta G^*_{E=E_0}$ is the activation energy at the potential for the onset of adsorption of oxygen species on the platinum surface at pH = 0. Combining the equations yields

$$\Delta G^*_\theta = \Delta G^*_{E=E_0} + \alpha FE + 2.3\alpha RT\text{pH} \tag{7}$$

If one then postulates the rate-determining step (involving an electron transfer, pH dependence, and the adsorption of an oxygen species) to be

$$S + O_2 + H^+ + e^- \longrightarrow S - O_2H \tag{8}$$

Then the resulting rate equation in the Tafel regime will be

$$i = k'nFp_{O_2}[H^+]\exp\left[\frac{-\Delta G^*_\theta}{RT}\right]\exp\left[\frac{-\beta FV}{RT}\right] \tag{9}$$

Substituting equation (7) and assuming that $\alpha \approx \beta \approx 0.5$ yields

$$i = knFp_{O_2}[H^+]^{1.5}\exp\left[\frac{-FV}{RT}\right] \tag{10}$$

This is in good agreement with the experimentally observed results. The same mechanism can also be used at lower potentials (higher current densities), where the total coverage of oxygen species is expected to be small. With no potential dependent coverage of surface oxygen species, and again assuming that $\beta \approx 0.5$, reaction (8) will yield the observed Tafel slope of $-120\,\text{mV decade}^{-1}$, and the reaction orders of one with respect to oxygen pressure, and one with respect to pH.

It should, however, be noted that equation (8) can be broken down into

$$S + O_2 \longrightarrow S - O_2 \text{ (fast)} \tag{11}$$

and

$$S - O_2 + H^+ + e^- \xrightarrow{\text{rds}} S - O_2H \tag{12}$$

and that other possible products could be envisioned such as SO + SOH without changing these relationships.[16]

While the initial work was done in acidic solutions, the approach was later extended to higher pH values where some changes were observed.[16, 18] Notably, an Tafel slope of $-60\,\text{mV decade}^{-1}$, and reaction orders of one with respect to oxygen pressure, and 0.5 with respect to pH at low current densities were observed. At high current densities (where little coverage of the platinum surface with oxygen species occurs), the observed Tafel slope is $-120\,\text{mV decade}^{-1}$, the reaction order is one with respect to oxygen pressure, and there is no dependence on pH. This was explained using the same approach as before (involving interactions with a partial coverage of oxide at low current densities), but using a pH independent rate-determining step of

$$S + O_2 + e^- \longrightarrow S - O_2^- \tag{13}$$

or

$$S + O_2 + H_2O + e^- \longrightarrow S - O_2H + OH^- \tag{14}$$

(with other products possible, as was mentioned for acidic solutions).

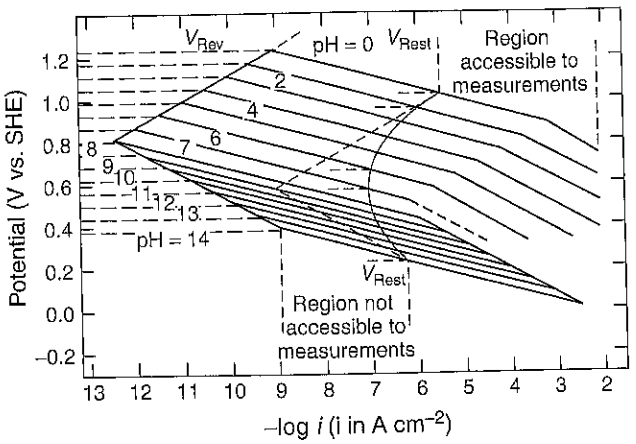

Figure 6. Diagram based on the developed model, showing the polarization curves for oxygen reduction on platinum for the entire pH range. (Reproduced from Sepa *et al.* (1981)[20] by permission of Elsevier Science.)

Using these rate equations, a diagram can be developed for the current-potential response for oxygen reduction at the platinum electrode as shown in Figure 6.

It should also be recognized that other data sets and explanations have been developed over the years,[4, 19] but at the present time this appears to be the most internally consistent approach,[18] which also encompasses a large range of data. Finally, as was mentioned earlier, establishing information about the reaction beyond the rate-determining step requires the application of other techniques.

2.3.2 *Isotopic results*

Studies using isotopic oxygen have been useful in examining the reactions of molecular oxygen and hydrogen peroxide.[4] Using mixtures of ^{18}O–^{18}O, ^{18}O–^{16}O, and ^{16}O–^{16}O on various surfaces, it has been shown that, for the reduction of oxygen to peroxide, the oxygen atoms are not exchanged. This underlines the stability of the O–O bond.

In addition, little exchange of the oxygen is found during heterogeneous decomposition of peroxide to oxygen at a platinum surface.[4] The degree of exchange in this peroxide decomposition reaction increases in the presence of alkali earth cations, and decreases with the presence of Cl^- or $H_2PO_4^-$. This was interpreted in terms of two mechanisms for the peroxide decomposition. One involves the direct interaction between two peroxide molecules (which can lead to an exchange of oxygen) and the other involves coupled electrochemical reactions via the electrode surface (which results in an oxygen without breaking of the O–O bond).

2.3.3 *Rotating ring disk electrode results*

In trying to study the reaction intermediates of oxygen reduction, the rotating ring-disk electrode (RRDE) method of Frumkin *et al.*,[21] has been an important tool. It was first applied to the investigation of the oxygen reduction reaction by Mueller and Nekrasov,[22] and still continues to be used. Many attempts have been made to use the data resulting from RRDE studies to obtain insight into the reaction pathways at the electrode surface.

The RRDE can detect the amount of peroxide released into solution in relation to the total reaction occurring at the disk electrode. This can be seen in Figure 7 where the disk and ring currents are shown as functions of potential. It can be seen that, at potentials below about 0.15 V, the number of electrons involved in the oxygen reduction at the disk decreases, and peroxide is detected at the ring. This is thought to be due to an interference effect of the adsorbed hydrogen on the oxygen reduction reaction, although a reaction between the oxygen reduction intermediates and adsorbed hydrogen has also been suggested.

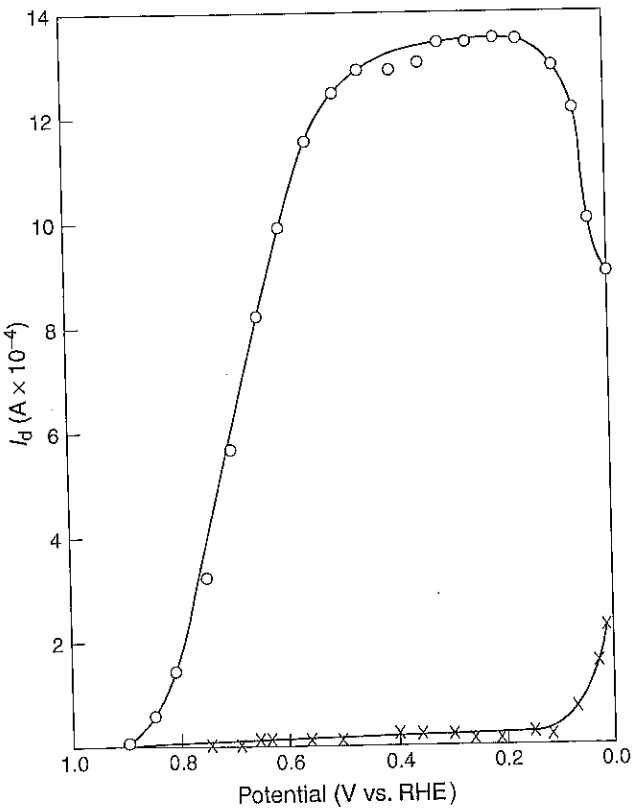

Figure 7. RRDE currents for oxygen reduction at platinum; o disk current, and x ring current. (0.1 N H_2SO_4, $\omega = 120\,s^{-1}$, ring at 1.4 V vs. RHE). (Reproduced from Damjanovic *et al.* (1967)[23] by permission of The Electrochemical Society, Inc.)

This example illustrates how the RRDE allows one to distinguish between 2- and 4-electron reductions. It does not directly allow one to distinguish between a parallel 4-electron reduction and a 4-electron reduction via peroxide. Therefore a significant amount of work has focused on examining the dependence of the RRDE response with rotation rate and disk potential to try to obtain more information. Various reaction pathway models have been developed and their expected responses evaluated, then compared to experimental data. This approach has to be used with care, however, because any number of mechanisms may be able to fit a given set of data.

An initial approach (Scheme 1) was described by Damjanovic *et al.*, that distinguished between the series mechanism (through peroxide ($k_2 + k_3$)) or the parallel mechanism (with earlier breaking of the oxygen bond then reduction of the two fragments to water (k_1)).[24]

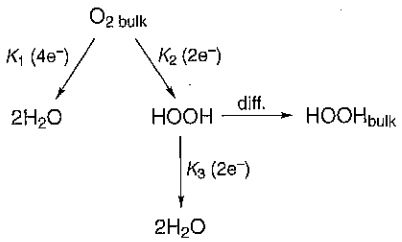

Scheme 1

At steady state, the rate equations can be solved to yield

$$\frac{I_D}{I_B} = \frac{I_D}{(I_R/N)} = \left(\frac{4k_1}{2k_2} + 1\right) + \left(\frac{4k_1}{2k_2} + 2\right) k'\omega^{-1/2} \quad (15)$$

where I_D is the disk current, I_R the ring current, N the ring collection efficiency, I_B the ring current corrected for the collection efficiency, ω the RRDE rotation rate, and $k' = 1.61D^{-2/3}\nu^{1/6}k_3$ (where D is the diffusion coefficient of peroxide and ν is the solution kinematic viscosity). The rotational dependence of the ring-disk data was then used to distinguish between the different pathways using a plot of I_D/I_B versus $\omega^{-1/2}$.

It should be noted, however, that the relationships derived are based on the assumption that the rate of release of peroxide from the disk is governed by mass transport, which results in its dependence on rotation rate. If this is not the case, due for example to desorption-controlled release of the peroxide, the intercept at infinite rotation rate will be more complicated and the results of the I_D/I_B versus $\omega^{-1/2}$ plots more difficult to interpret. Thus this model is not sufficiently general, and by not including such reaction steps as peroxide decomposition, and the adsorption and desorption of reactants and products, the results of an analysis with this model (and other simplified models) will reflect the starting assumptions. Unfortunately, it has been shown that for more general models, there is insufficient data available to determine all the rate constants.[25] Accordingly, different simplified models have been used for specific electrode materials, and data on the electrochemistry of peroxide solutions has also been used to try to determine some of the constants. Listings and comparisons of the models can be found elsewhere.[4, 7, 9, 26] In addition, work has been done to develop diagnostic criterion in the form of plots, which can be used to compare the relative rates of different reaction pathways.

A commonly used plotting method was developed by Wroblowa *et al.*, for the proposed reaction pathways, shown in Scheme 2.[27]

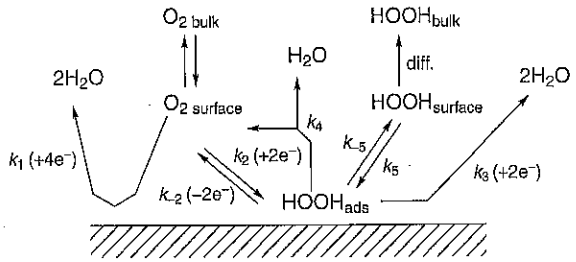

Scheme 2

This scheme does not explicitly include an $O_{2\,ads}$ species (essentially lumping together the $O_{2\,surface}$ and $O_{2\,ads}$, which is mathematically equivalent to assuming a rapid equilibrium between $O_{2\,surface}$ and a low coverage of $O_{2\,ads}$). For this scheme, the resulting equations are

$$\frac{I_D}{I_B} = \frac{I_D}{(I_R/N)} = 1 + 2\frac{k_1}{k_2} + A + \frac{k_5}{\gamma_A \omega^{1/2}} A \quad (16)$$

where

$$A = \left(\frac{2k_1}{k_2 k_{-5}}\right)(k_{-2} + k_3 + k_4) + \frac{(2k_3 + k_4)}{k_{-5}} \quad (17)$$

and

$$\gamma_A = -0.62D^{2/3}\nu^{-1/6} \quad (18)$$

It was noted that for an I_D/I_B versus $\omega^{-1/2}$ plot of these equations, the intercept (J) at infinite rotation rate would be given by

$$Intercept = J = 1 + 2\frac{k_1}{k_2} + A \quad (19)$$

and the slope (S) by

$$Slope = S = \frac{k_5}{\gamma_A} A \tag{20}$$

Then for a series of curves measured at different potentials, the intercepts and slopes can be related by

$$J = 1 + 2\frac{k_1}{k_2} + \frac{\gamma_A}{k_5} S \tag{21}$$

The resulting $J-S$ plots provide an additional method for viewing data. If k_1 and k_2 have the same potential dependence and if k_5 is potential independent, a linear plot with an intercept of $(1 + 2k_1/k_2)$ will result. This intercept can be used to find the ratio of k_1 (the parallel mechanism) to k_2 (the series mechanism). If k_1 and k_2 have different potential dependencies, the plot will appear curved.

An example of such a plot is shown in Figure 8 for oxygen reduction in 85% phosphoric acid.[28] The straight line relationships in the I_D/I_R plot confirm that the reaction is first order in oxygen. The straight line $J-S$ plot indicates that k_1 and k_2 have the same potential dependency with the intercept $(1 + 2k_1/k_2)$ of 5.2 giving an estimate of k_1/k_2 of 2.1. On gold, $J-S$ plots show an intercept of close to one, indicating that k_1 is essentially zero,[27] and for platinum in 0.55 M H_2SO_4 a curved plot is reported, indicating (according to the model) different potential dependencies for k_1 and k_2.[26]

In the latter paper, a comparison of some simplified models was made and it was concluded that, for their case, the model of Damjanovic was adequate. Then, using a combination of I_D/I_B versus $\omega^{-1/2}$ and $I_{Dlim}/(I_{Dlim} - I_D)$ versus $\omega^{-1/2}$ plots, values of k_1, k_2 and k_3 were obtained at various potentials. These results are shown in Figure 9. The parallel route dominates ($k_1 \gg k_2$) from about 0.8–0.6 V RHE. However, below about 0.6 V, k_1 becomes potential independent (which corresponded to an observed flattening of the mass transfer corrected Tafel slope) leading to speculation about an oxygen adsorption or chemical rate-determining step before the first electron transfer. At very low potentials (around 0.4 V), the series pathway begins to dominate, though k_3 remains larger than k_2 and so most of any peroxide produced would be expected to be further oxidized to water.

A very general reaction pathway has been developed by Anastasijevic *et al.*[29] (see Scheme 3: modified for acid conditions for ease of comparison with the other schemes). This scheme is written using only single electron transfer steps, and explicitly includes oxygen irreversible dissociative adsorption at sites for strong adsorption, versus weak adsorption sites for the series route. It also allows for transfer of series pathway intermediates at weakly adsorbing sites to strongly adsorbing sites of the parallel pathway, effectively blurring the difference between a series and parallel route. They found when using the more general model that interpretation of the various plots was more complex, but a number of conclusions could

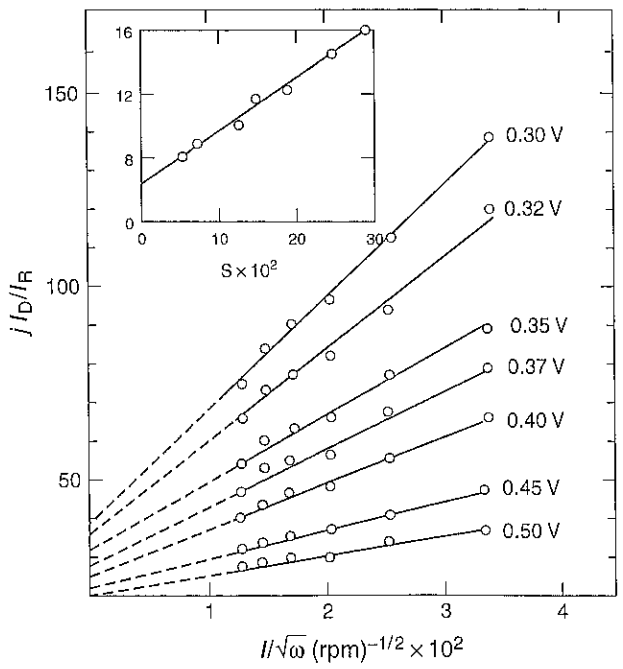

Figure 8. I_D/I_R versus $\omega^{-1/2}$, and $J-S$ plots for oxygen reduction on platinum. (85% H_3PO_4, 25 °C, ring potential 1.2 V, voltages versus RHE, N = 0.40). (Reproduced from Adzic (1998)[9] by permission of Wiley-VCH.)

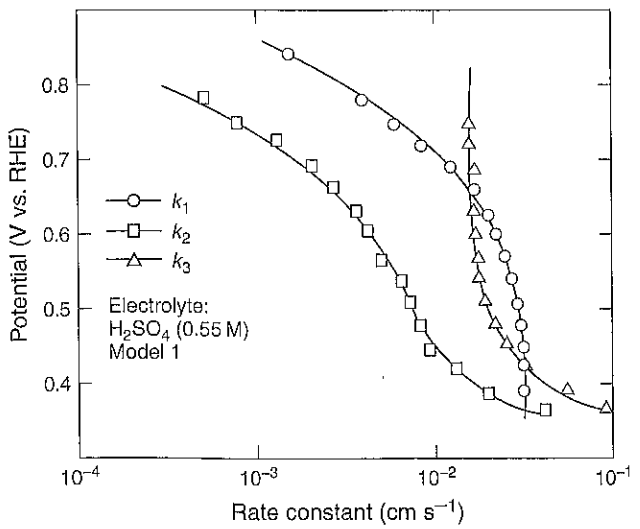

Figure 9. Rate constants for the intermediate steps of O_2 reduction on Pt as a function of potential. Constants calculated based on Scheme 1. (0.55 M H_2SO_4, 25 °C). (Reproduced from Hsueh *et al.* (1983)[26] by permission of Elsevier Science.)

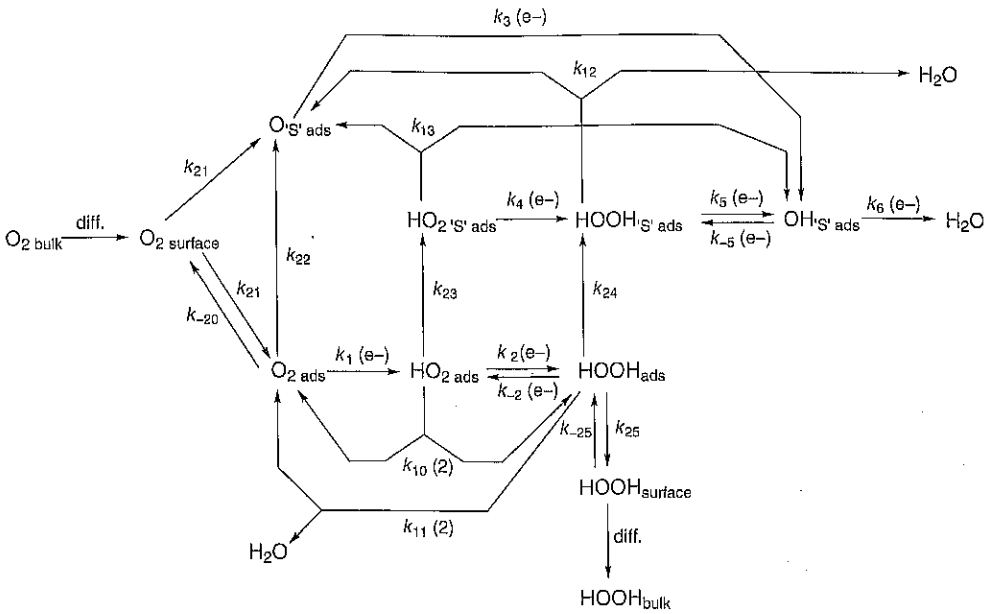

Scheme 3

still be drawn.[29] A linear I_D/I_B versus $\omega^{-1/2}$ plot is characteristic of a pathway with first order (or pseudo first order) elementary reaction steps that produces only one compound that reacts at the ring. Non-linear $J-S$ plots are characteristic of coupled series and parallel pathways (i.e., k_{22} and/or $k_{23} > 0$). A linear $J-S$ plot with an intercept greater than $2/n_R$ (where n_R is the average number of electrons exchanged per oxygen) implies that a parallel pathway is operating and the ratio of parallel to series path can be estimated. And the $J-S$ plot consists of a single point when only the 2-electron series pathway is operating. Finally, while fitting such a complex model does not seem possible using electrochemical data alone, simplified models must be used with caution to avoid misleading conclusions that can be made using a model that overlooks possible reaction intermediates or steps. Nevertheless, some useful qualitative and quantitative information can be obtained.

The concept of different sites for the parallel 4-electron and series 2- and/or 4-electron reductions of oxygen has developed from numerous experiments over the years. These experiments have shown the non-equivalent influence of adsorbed and sub-monolayer deposits of species (under potential deposition (UPD) metals or partially reduced oxides) on the two reactions.[4, 9] In general on platinum, while such species tend to inhibit the overall reduction of oxygen, they more strongly inhibit the parallel reaction pathway. An example of such work is shown in Figure 10. This work shows the influence of different anions on the RRDE response at a palladium electrode (which behaves generally similarly to platinum). It can be seen that in the presence of anions such as $H_2PO_4^-$, Cl^-, and Br^-, the overall process of oxygen reduction at the disk decreases, but the amount of peroxide oxidized at the ring increases.[30] This data was also examined in terms of a reaction pathway model (similar to Scheme 2) and it was found that these results were related to a decrease in k_1/k_2 (rather than simply a decrease in k_3). One explanation for this is that the parallel mechanism requires two adjacent sites for dissociative adsorption, while oxygen reduction to peroxide may only require one site. This would have the general effect of making the 4-electron reduction second order in available sites, and so be more sensitive to changes in the number of available sites.[4]

With the ability to prepare good quality single crystal RRDEs, these approaches are now being extended to investigating the effects of surface structure on the oxygen reduction reaction pathways.[9, 31] This work has confirmed the important role of structure-sensitive adsorption of anions. Adsorbed hydrogen (in the H_{UPD} region) decreases the disk current and quantitatively increases the ring current, which is felt to be due to a blocking of sites for breaking of the O–O bond.[31] On the other hand HSO_4^- was found to inhibit O_2 reduction, but not to affect the

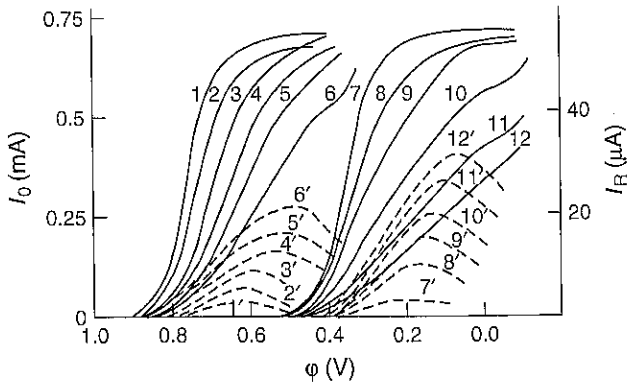

Figure 10. RRDE results for oxygen reduction at a Pd electrode showing the effect of adsorbed anions. 1: 0.1 N H_2SO_4, 2: 0.1 N H_3PO_4, 3–6: 0.1 N H_2SO_4 + HCl, 7–12: 0.1 N H_2SO_4 + HBr; at concentrations of: 7: 10^{-8} N, 8: 10^{-7} N, 9: 10^{-6} N, 3 and 10: 10^{-5} N, 4 and 11: 10^{-4} N, 5 and 12: 10^{-3} N, 6: 10^{-2} N. 1–12: disk current, 1′–12′ ring current, curves 7–12 and 7′–12′ are displaced by 0.2 V along the potential axis. (Voltages versus RHE). (Reproduced from Vilinskaya and Tarasevich (1973)[30] by permission of Kluwer Academic/Plenum Publishers.)

reaction pathway, as no peroxide was detected at the ring. It was also reported that on Pt(111), where irreversible PtOH formation does not occur until higher potentials, no change in Tafel slope at low current densities is observed, in keeping with the previously described theory. Single crystal investigations is discussed in detail in **Oxygen reduction reaction on smooth single crystal electrodes**, Volume 2.

2.3.4 *Gas phase adsorption data*

Gas phase studies of oxygen adsorption on platinum show strong interactions and dissociative adsorption. On Pt(111), true physisorption is found below 90 K, with the oxygen molecule sitting parallel to the surface. With increased thermal activation, chemisorption occurs with two different adsorbed states being found. One is a superoxide-type species (i.e., O_2^-) that is weakly bound, receiving one electron from the platinum surface in its π antibonding orbital. The other adsorbed state, reported to occur at higher temperatures (above 135 K) or at specific sites, is a peroxy-type species (i.e., O_2^{2-}) with two electrons donated by the platinum surface. Above about 100–150 K (or if other forms of activation energy are supplied) the chemisorbed species dissociate to atomic oxygen sitting at three-fold hollow sites (a (2 × 2) low energy electron diffraction LEED pattern).[32] The atomically adsorbed oxygen can be imaged by scanning tunneling microscope (STM) as can be seen in Figure 11. An interesting result is the non-uniformity of the oxygen adsorption, with the molecules dissociatively adsorbing to form clusters and chains.

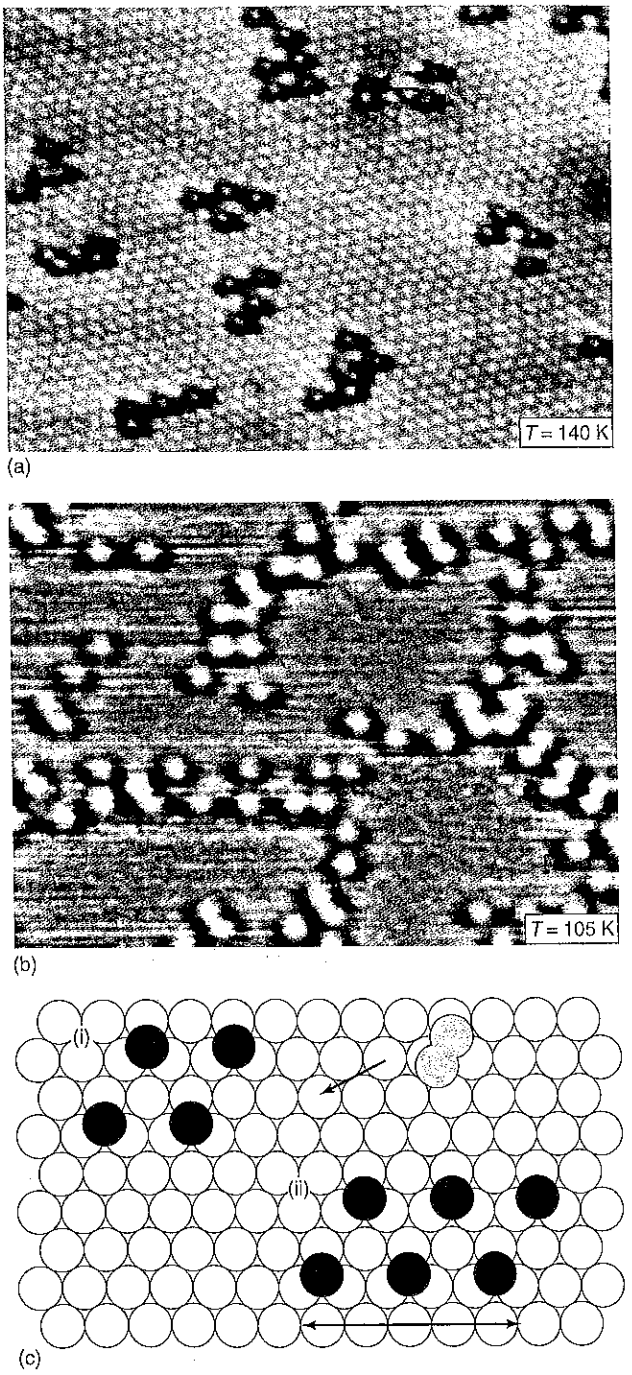

Figure 11. Atomic-resolution images of oxygen islands. The images illustrate the enhanced precursor dissociation probability at adsorbed oxygen atoms and the resulting quasi-one-dimensional growth for (a) T = 140 K (3 L dose, image 100 × 60 Å^2); (b) T = 105 K with chain-like islands corresponding to strings of oxygen pairs (1 L dose, image 70 × 40 Å^2); (c), Model illustrating the directional growth of O_{ad} (black spheres) chains on Pt(111); (i), an oxygen precursor molecule (shaded) approaches an atom island; (ii), on its dissociation a chain segment evolves. (Reproduced from Zambelli *et al.* (1997)[33] by permission of Nature Publishing Group.)

The dissociative adsorption is generally thought to pass through the same stages as seen on elevating the temperature. That is, the oxygen molecule physisorbs, and then passes through a chemisorbed oxygen molecule precursor or precursors, before dissociating at favorable sites. Based on ab initio local-spin-density calculations, the two chemisorbed molecular precursors are thought to be adsorbed in a bridge configuration between two Pt atoms (corresponding to the O_2^- type species), and asymmetrically across a three-fold hollow (see Figure 12) (corresponding to the O_2^{2-} type species).[34] The lowest energy dissociation path calculated for the latter species is diagrammed in Figure 12, leading to the atomic oxygen sitting at face centre cubic (FCC) sites with a final saturated coverage of one oxygen atom per four platinum surface atoms. The bridge type configuration is predicted to pass through the three-fold hollow type configuration as it dissociates. The key factor in the adsorption behavior is the interaction between the oxygen molecule antibonding orbital and the metal d band. This is influenced by the height of the metal d band relative to the Fermi level, and the interatomic spacing of the metal atoms relative to the oxygen molecule bond length.

While this provides background information about the interactions of oxygen with platinum, the electrochemical case will be more complex because of the presence of adsorbed water and ions, and of platinum hydroxide species coming from the oxidation of water. It is also interesting to note that the maximum coverage for gas phase adsorption is only 0.25 monolayers, and no equivalent process to place exchange is reported (at least until about 900 K where phase oxide formation begins).[35]

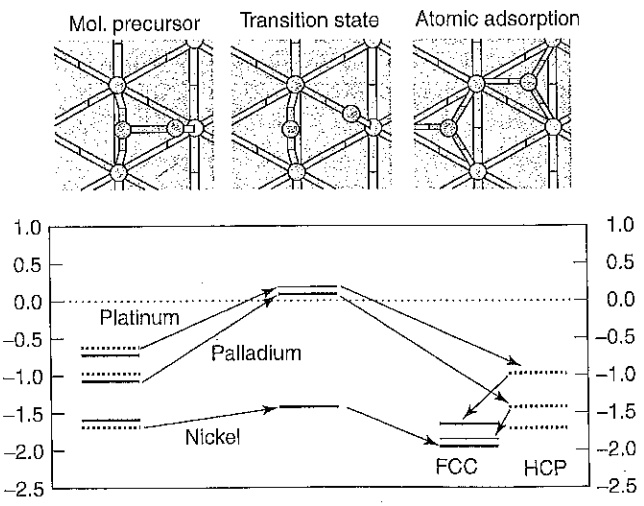

Figure 12. Sketch of the initial, transition, and final states for the dissociative adsorption of O_2 over Ni, Pd, and Pt(111). The initial state is the precursor over the hollow position [FFC (solid line) for Pt and Pd, hexagonal close packing (HCP) (dashed lines) for Ni] and then O_2 dissociated via the transition state into the again hollow adsorbed oxygen atoms [FFC (solid line) for all surfaces; for palladium and platinum the HCP site (dashed line) has to be crossed]. (Reproduced from Eichler *et al.* (2000)[34] by permission of the authors.)

2.3.5 *Molecular calculations*

The complexity of the oxygen reduction reaction makes fundamental modeling difficult. In one recent model, a single platinum site was used for coordinating the reactant species, along with an associated proton which was represented by a hydronium ion solvated with two waters.[36] The effect of electrode potential was considered by geometric variations to the reactant complex to achieve the desired electron affinity. This resulted in estimates of the transition state structure and its activation energy.

The reaction steps used were

$$Pt - O_2 + H^+_{(aq)} + e^- \longrightarrow Pt - OOH \quad (22)$$

$$Pt - OOH + H^+_{(aq)} + e^- \longrightarrow Pt(OHOH) \quad (23)$$

$$Pt(OHOH) + H^+_{(aq)} + e^- \longrightarrow Pt - OH + H_2O \quad (24)$$

$$Pt - OH + H^+_{(aq)} + e^- \longrightarrow Pt - OH_2 \quad (25)$$

It was found that, due to the donation of charge from the Pt to the oxygen atoms, the activation energy for formation of the transition states was greatly reduced for all steps except the reduction of the hydroxide radical, for which it increased. This shows how, while a strong metal oxygen interaction can facilitate the oxygen dissociation, too strong an interaction will inhibit the overall reaction. As well as step (23), an alternative step (shown below step (26)) was also considered, but excluded because of its high activation energy.

$$Pt - OOH + H^+_{(aq)} + e^- \longrightarrow Pt - O + H_2O \quad (26)$$

The calculated energies for the various intermediates and their transition states are plotted as a function of applied potential along the reaction pathway in Figure 13. It can be seen that the highest activation energy is predicted to be for the dissociation of peroxide, implying that peroxide would be the principle product with the initial electron transfer to adsorbed O_2 being the rate-determining step. Hence these results suggest that single Pt sites with end-on O_2 adsorption would favor peroxide formation, hence O–O bond cleavage and 4-electron reduction probably requires two or more free adjacent Pt sites.

This provides some confirmation of the suggestion by Yeager that the reaction pathway varies depending on the mode of O_2 adsorption. End-on adsorption (Pauling type) was thought to favor peroxide formation, and side-on

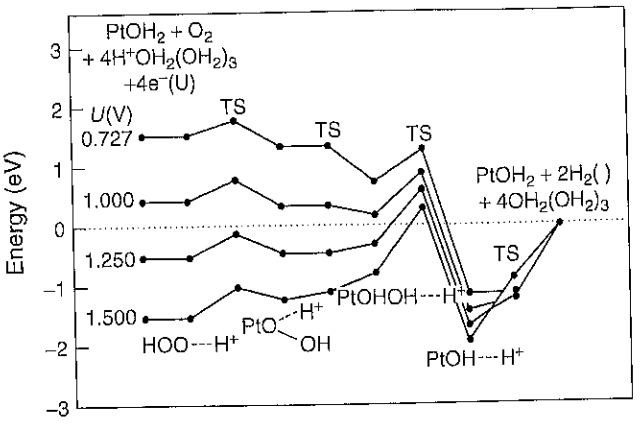

Figure 13. Energies as functions of electrode potential for the O_2 reduction reaction system passing through the peroxide pathway. TS = transition state. (Reproduced from Anderson and Albu (2000)[36] by permission of The Electrochemical Society, Inc.)

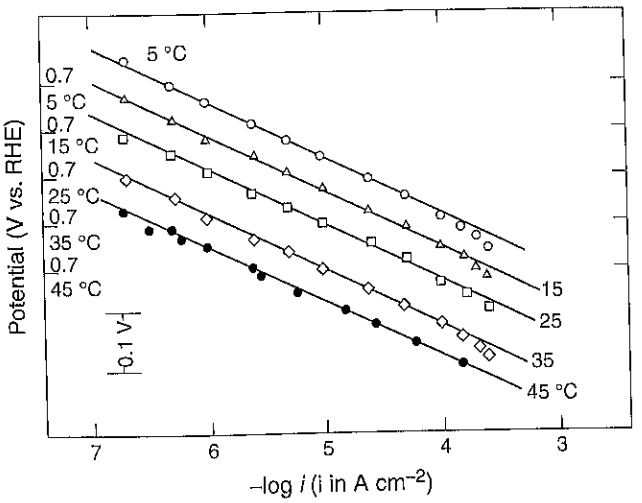

Figure 14. Tafel relationships at Au electrodes at different temperatures. (pH 2.2 $HClO_4$, RHE reference at room temperature). (Reproduced from Damjanovic *et al.* (1986)[37] by permission of Berichte der Bunsen-Gesellschaft für Physikalische Chemie.)

adsorption (either at a single site (Griffiths type) or across two sites (bridge type)) was suggested to lead to water.[9]

3 EFFECT OF TEMPERATURE

Different results have been reported for the temperature dependence of the oxygen reduction reaction. Depending on the electrode type, the electrolyte, and whether the electrode is reduced or oxide covered, temperature independent or temperature dependent Tafel slopes have been reported.[6] An example of a temperature independent Tafel slope is shown in Figure 14. As well as raising questions about the characteristics of the electron transfer, this effect complicates the determination of the heat of activation for the reaction.

A framework for characterizing these anomalous transfer coefficient dependencies has been developed by Conway,[38] and has been discussed for the case of oxygen reduction.[39, 40] Starting from the standard Gibbs energy of activation at a given electrode potential V, offset from a reference potential

$$\Delta\overline{G}^{*} = \Delta G_0^{*} + \beta F V \tag{27}$$

where ΔG_0^{*} is the standard Gibbs energy of activation at the reference potential. Ideally the reference potential would be the potential of zero Galvani potential difference ($\Phi^{M} = \Phi^{S}$), however, as this is not known, an apparent energy of activation is customarily defined at the reversible potential (ΔG_a^{*} or ΔG_R^{*}). The value β (the symmetry factor) is the fraction of the electrode potential influencing the activation energy and so

$$\beta = \frac{1}{F}\frac{\partial\Delta\overline{G}^{*}}{\partial V} = \frac{1}{F}\frac{\partial\Delta\overline{H}^{*}}{\partial V} - \frac{T}{F}\frac{\partial\Delta\overline{S}^{*}}{\partial V} \tag{28}$$

where ΔH^{*} and ΔS^{*} are the enthalpic and entropic components of the Gibbs energy of activation at a given electrode potential. One can then make the simplifying assumptions that the derivatives with respect to the enthalpic and entropic components are constant over the range of potential and temperature of interest. (The empirical nature of this approach was pointed out by Gileadi).[41] Then β can be written as

$$\beta = \beta_H + T\beta_S \tag{29}$$

In this manner β can be expanded into a temperature dependent and a temperature independent component. Experimentally the constants can be determined using a Conway plot of reciprocal Tafel slope versus $1/T$.

It should be noted that while equation (29) has been derived for the symmetry factor, more than simply an electron transfer will be involved for most reactions, and so the measured variable will be a transfer coefficient (α). This is important because more complex reaction schemes may result in other terms in the rate equation due to, for example, adsorption (a θ or $(1-\theta)$ term). Though for such a factor to affect the Tafel slope in a manner that changes with temperature, it would have to be both potential and temperature dependent.

In general, for oxygen reduction at oxide-free metal electrodes (such as Pt, Pd, and Rh) in aqueous solutions, β is

approximately constant (β_H is between 0.4 and 0.5 and β_S is small and around $2 \times 10^{-4}\,K^{-1}$(or possibly even zero)[31]). In contrast, at oxide covered electrodes the Tafel slope is essentially constant and β therefore varies linearly with temperature (hence β_H is close to zero). Such temperature-independent Tafel slopes have also been reported for gold (as shown in Figure 14), and for some conditions with Pt in concentrated phosphoric acid.[40, 42]

Small variations of the entropy of the activated complex with potential are conceivable (i.e., a non-zero value of β_S). However, a complete lack of effect of changing the enthalpy of the product (by changing the potential), on the enthalpy of an activated complex located at a state midway between the reactant and the product, is difficult to understand (i.e., a β_H of close to zero). (This is especially true when one considers that at the same time the entropy of the activated complex is supposed to be changing).[41] In fact, it is recognized that the cases that yield a β_H of close to zero represent complex electrochemical situations.[38] In particular, this is true at oxide-covered electrodes, where the state of the oxide and the related position of the activated complex in the applied electric field can easily vary with temperature and potential. (Extreme anomalous temperature dependence (i.e., a β_H of close to zero) is also commonly found for oxygen evolution at oxide-covered electrodes). For the case of results obtained in concentrated media, such as phosphoric acid, Appleby has suggested a change in available sites as a function of potential and temperature, due to changes in the adsorption of oxygen species at the electrode surface.[5] It has also been pointed out that insufficient information is available to properly correct for diffuse double layer effects in media such as concentrated phosphoric acid.[43] It has also been suggested that the oxygen reduction mechanism in concentrated phosphoric acid may differ from that indicated by equations (11) and (12).[40] The case of gold is puzzling, but may be related to the large variations of activities (and Tafel slopes) found on different crystal faces.[44] It has been shown that, in some circumstances, two parallel reactions can give a total current that has the appearance of a temperature-independent Tafel slope.[45] A summary of proposed explanations was made by Yeager,[40] based on Conway's review of the area.[46] These include:

(a) tunneling in reaction coordinate space;
(b) potential and temperature dependent:
  (i) surface adsorption/desorption of the reactants;
  (ii) changes in the structure of the double layer (particularly solvent structure and double layer thickness);
  (iii) or adsorption/desorption of charged species from the supporting electrolyte, resulting in changes in the activity coefficient of the activated state;
(c) changes in the symmetry of the potential energy barrier;
(d) partial drop of the electric field at the electrochemical interface within the electrode phase;
(e) a shift in the rate-determining step;
(f) artifacts due to impurities.

Some of these explanations are overlapping, and with many of them it would be difficult to explain a complete independence of the Tafel slope with temperature, unless the effects were so large as to be more commonly observed. Some of these effects have been estimated and are expected to not be large, with β_S values of less than $1.5 \times 10^{-3}\,K^{-1}$.[47] Further, in some cases, such effects would also be expected to result in a potential dependence of the Tafel slope.[43]

Finally, it should be noted that a series of precise studies has been carried out investigating the anomalous temperature dependence of transfer coefficients. In most cases studied to date, after careful double layer corrections, the apparent temperature dependent transfer coefficients have been found to disappear. However, in one recent study an apparent true variation of the transfer coefficient has been found.[43]

One result of these discussions impacts the evaluation of the apparent heat of activation at the reversible potential (ΔH_R^*). If this is calculated by extrapolation of heats of activation measured at other potentials, the data should be corrected using β_H rather than β (as follows from equations (28) and (29)). A second result is that when β_H is zero, care should be taken in using the Tafel slope for mechanistic determinations. Under such a situation the reaction, and the environment at the electrode surface, are probably complex.[41, 48]

Evaluation of apparent heats of activation has proven useful in the understanding of the oxygen reduction reaction. Extrapolation of the measured heats of activation for oxygen reduction on Pt from the low and high current regions to a common potential was able to show the same apparent heat of activation.[49] This supports the hypothesis that the basic mechanism is the same in both regions (equation (8) in acid and equations (13) or (14) in base). More recently, equal apparent heats of activation for oxygen reduction at different platinum crystal faces has been used to support the idea that the same reaction pathway occurs on all the tested faces.[31]

4 OTHER ELECTRODE MATERIALS

Oxygen reduction is a surface-sensitive reaction and so the electrode material will strongly affect the reaction. Two classes of materials can be identified based on whether predominately a 2-electron or 4-electron reduction occurs.[4, 48]

Differences in oxygen bonding will affect the reaction pathways on different metals. Materials that weakly interact with oxygen would therefore be expected to favor the two electron reduction to peroxide. Those with stronger oxygen interactions can dissociate the oxygen molecular bond allowing the formation of water.

Predominantly 2-electron reduction to peroxide (O–O bond not broken):

- mercury
- gold (except gold (100) in alkaline solution)[50]
- carbon
- oxide covered metals
- most transition metal oxides.

Predominantly 4-electron reductions occur (O–O bond broken):

- platinum
- platinum family metals
- platinum alloys
- silver
- gold (100) in alkaline solution[50]
- metallic iron in neutral solution[9]
- some oxides (pyrochlores).

Of these materials, for fuel cells operating with acidic electrolytes, platinum and its alloys are commonly used, with carbon being used as a supporting material. In alkaline systems a wider variety of electrode materials is possible. Platinum, its alloys, and silver can also be used. In addition, two electron reduction materials can be combined with peroxide decomposition catalysts such as silver, platinum, or various transition metal oxides. The decomposition catalysts ideally keep the concentration of peroxide within a fuel cell electrode structure close to zero and regenerate oxygen, thus allowing an overall 4-electron reaction to occur. In the alkaline case, the carbon support is also an active part of the electrode. (Alkaline fuel catalysts is discussed further in **O_2 reduction and structure-related parameters for supported catalysts**, Volume 2)

The two electron reduction of oxygen will yield peroxide. This is a kinetically easier reaction than the reduction to water, and so the reverse reaction of oxidation of peroxide to oxygen can be studied without greatly changing the potential (and so at a similar electrode surface). In theory this can be used to provide additional information about the reaction mechanism, though in practice care must be taken to distinguish between currents for oxygen reduction, peroxide oxidation, and peroxide reduction, and due to peroxide decomposition (which releases oxygen at the electrode surface).

4.1 Gold

Gold is unique among the metals studied for oxygen reduction because of its lack of ability to adsorb oxygen (having no unpaired d-electrons), which is reflected in its high potential for oxide formation (1.457 V vs. SHE).[11] The average number of electrons transferred per oxygen molecule during its reduction has been reported to vary with potential and crystal face. The Au(100) face in particular shows high (4-electron) catalytic activity in the region in alkaline solution where surface adsorbed AuOH exists.[44] The reactions at gold can be complex, with oxygen reduction, peroxide reduction, peroxide oxidation, and peroxide decomposition all possibly occurring, depending on the potential and crystal face. Intermediates therefore can also be expected to diffuse between sites of different activities. Its activity can also be greatly enhanced by impurities, especially in acid solutions where oxygen reduction is very slow. This has been most notably reported for platinum ions corroded from other electrodes in the electrochemical cell.[4]

In general, oxygen reduction on gold is found to be first order in O_2, pH independent, and yielding a Tafel slope of around $-120\,\mathrm{mV\,decade^{-1}}$ (the latter shown in Figure 14).[6, 51] Therefore the rate determining step is considered to be

$$S + O_2 + e^- \longrightarrow S - O_2^- \qquad (30)$$

However, in some cases the initial adsorption (before the electron transfer) has been felt to be the rate-determining step.[4] In alkaline media, the reverse reaction of peroxide oxidation has been studied and reported to be 1/2 order with respect to OH^- and HO_2^-, and the Tafel slope was $-120\,\mathrm{mV\,decade^{-1}}$. This has led to the overall second stage of the reaction (itself involving a few steps), being postulated to be[51, 52]

$$2S - O_2^- + H_2O \longrightarrow 2S + HO_2^- + O_2 + OH^- \qquad (31)$$

though it should be noted that a clear reaction order of 1/2 with respect to HO_2^- was only obtained at higher overpotentials for peroxide oxidation. In the potential range for significant oxygen reduction, it has been suggested that the second step could become the further reduction of O_2^-[53]

$$S - O_2^- + H_2O + e^- \longrightarrow S - HO_2^- + OH^- \qquad (32)$$

More recent work has focused on the nature of the reaction at single crystals and the effects of ad-atoms and UPD metals.[9] The effect of potential cycling to *activate* polycrystalline gold foil for oxygen reduction has been

followed by STM, where it was found that a relatively well defined crystal surface with coherent areas of Au(100) can be formed.[54]

4.2 Carbon materials

The reduction of oxygen on carbon is catalyzed by strong interactions with the surface. While outer Helmholtz (non-interacting) reduction of oxygen to superoxide (O_2^-) has been reported to be possible at basal plane graphite, the rate is far lower than for oxygen reduction at other carbons.[48] In the same paper, it is also reported that the attachment (by pre-adsorption or chemical bonding) of various quinones to basal plane graphite, to simulate some of the functional groups found on the carbon surface, results in a large enhancement of the oxygen reduction current.

Slightly different mechanisms have been proposed by different workers, with one key difference being between results using graphite versus glassy carbon. The reaction is pH independent, and first order in oxygen. Tafel slopes are typically around $-120\,\text{mV decade}^{-1}$ for graphite and $-60\,\text{mV decade}^{-1}$ for glassy carbon, though variations around these values have been reported for different carbons, and values as low as $-30\,\text{mV decade}^{-1}$ have been reported in strong alkali (i.e., 6 N KOH).[55] Generally the first reaction step is thought to involve adsorption and electron transfer (similar to gold, see equation (30)). Following this, either further reduction or disproportionation (as in equation (31)) have been proposed.[56] A step involving a transformation between two different forms of adsorbed superoxide has also been proposed.[48] In alkaline solutions (pH > 10) two waves are seen in oxygen reduction polarization curves, both corresponding to oxygen reduction to peroxide, but most probably at different sites on the carbon surface.[57] Different cations, D_2O versus H_2O, and selective modification of different carbon surface groups, have all been reported to shift the oxygen reduction voltammetric wave.[56] All these factors confirm the complex role that carbon surface chemistry plays in the reaction, which should be taken into account when considering the oxygen reduction mechanism. Some of the important surface features of carbon are shown in Figure 15.

4.3 Iridium oxide

Oxygen reduction on iridium is of interest because of its possible application in regenerative fuels cells (see for example Ref. [59]). In the potential region of oxygen reduction, iridium electrodes are covered with a phase oxide. As a result, the electrode surface/solution interface

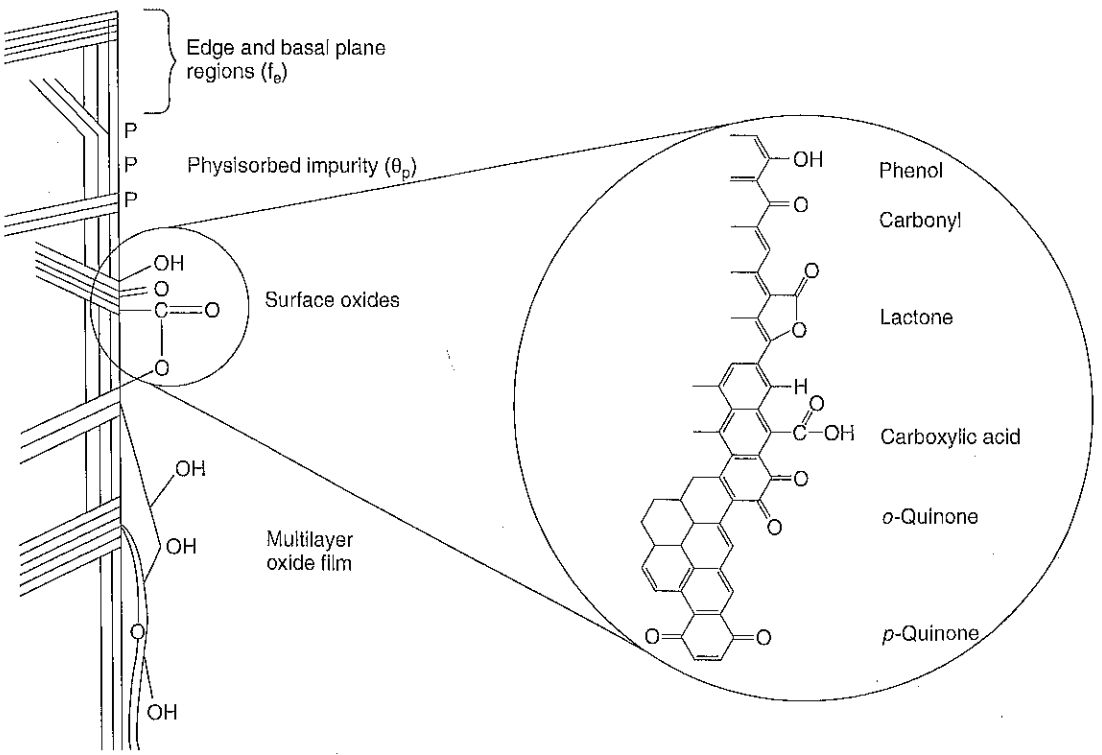

Figure 15. A schematic showing some of the carbon surface features of relevance to electrochemistry, and details of some different possible oxygen-containing surface functional groups. (Reproduced from McCreery (1991)[58] by permission of Marcel Dekker, Inc.)

will have an acid-base equilibrium and an associated potential difference.[60] Rate data shows a low current density and a high current density region, with the change occurring at about 1×10^{-5} A cm^{-2} independent of pH (see Figure 16).

In the low current region the reaction rate is given by[6]

$$i_l = k_l[H_3O^+]p_{O_2} \exp\left(\frac{-FE}{RT}\right) \tag{33}$$

and in the high current region by

$$i_h = k_h[H_3O^+]^{1/2}p_{O_2} \exp\left(\frac{-FE}{2RT}\right) \tag{34}$$

The fractional reaction order with respect to acid in the high current density region is explained by considering the potential field set up by the acid-base equilibria between the metal oxide and the solution (shown below in Figure 17).

The potential difference developed between the surface layer of the oxide and the solution is given by[60]

$$\Delta\phi^* = \text{const.} - \frac{2.3RT}{F}\text{pH} \tag{35}$$

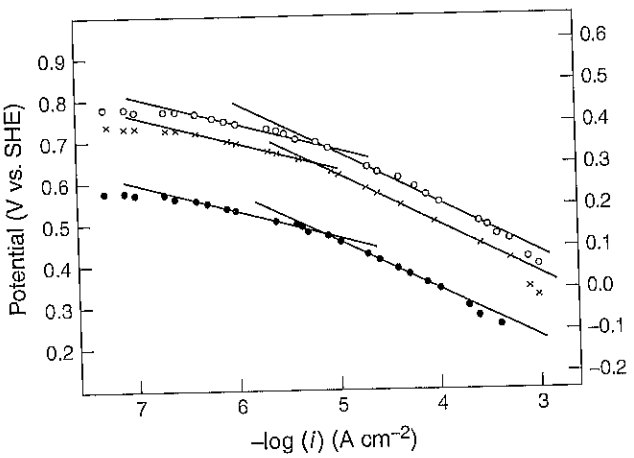

Figure 16. Polarization curves for oxygen reduction at an iridium electrode; ○ pH 2.2, × pH 3.1, and ● pH 11.0. (1 atm O_2, 25 °C). (Reproduced from Sepa *et al.* (1987)[61] by permission of Elsevier Science.)

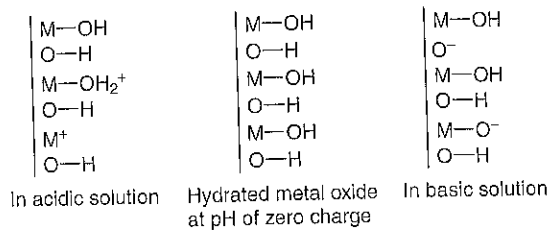

Figure 17. Schematic of the metal oxide solution interface in different pH regions (based on Ref. [60]).

One can then assume, for the high current density range, an initial electron transfer rate determining step as in equation (30) occurring in the inner Helmholtz layer (IHL). For such a case, only part of the applied potential difference will affect the reaction rate.

$$i_h = k_h[H_3O^+]p_{O_2} \exp\left(\frac{-\beta F(E - \Delta\phi^*)}{RT}\right) \tag{36}$$

substituting equation (35) in equation (36) yields

$$i_h = k_h'[H_3O^+]^{\beta}p_{O_2} \exp\left(\frac{-\beta FE}{RT}\right) \tag{37}$$

which for $\beta = 1/2$ will be identical to equation (34). In a similar manner, one can choose as rate-determining step a chemical step following the first electron transfer (which would then be in quasi-equilibrium). If the resulting rate equation is then corrected for the potential drop from the IHL to the solution, an equation of the form observed for the low current density region (equation (33)) results.[6] However, while this reaction model appears to fit the data, it has been shown to be overly simplified. This is because both Tafel slopes have been found to be unchanging with temperature (over a range from 5 to 45 °C).[62] As was discussed earlier, if β_H appears to be zero, this raises concerns that the present understanding of the system is insufficient. This is definitely true for the reaction rate in the low current density region, where a transfer coefficient of one is not expected to be temperature dependent.[62] Thus a complete understanding of oxygen reduction on metal oxide surfaces will require further study.

5 VOLCANO PLOTS

In attempting to correlate electrocatalytic ability with some physicochemical property of a material, plots can be made of electrochemical activity (either current density at constant potential, or potential at a constant current density) versus the physicochemical property under consideration. If the resulting plot shows a maximum in activity with roughly linear correlations on either side of the maximum, it is referred to as a volcano plot. These plots were first proposed for understanding catalysis data by Balandin.[63]

The optimum heterogeneous catalyst will provide the correct reaction site geometry, along with the proper electronic environment, to facilitate the reaction of interest. Following this, the reaction sites should allow easy release of the product to achieve a high rate of site turnover. The geometric properties considered can include the interatomic distance, the crystal structure, its grain size, and the concentration and types of defects and irregularities.

Electronic parameters can include the %d character, d-band vacancies, and more general characteristic measures such as the work function and the latent heat of sublimation. It is usually felt that the catalyst site should adsorb the reactant (for the rate determining step) sufficiently strongly to activate it (to lower the energy required to achieve the activated intermediate), but not so strongly as to stabilize the reactant.

A volcano plot based on the d-electron properties of various metals and alloys is shown in Figure 18. The plot shows clear trends even though, at the chosen potential, the metals considered include bare metals, partially oxide covered, and phase oxide covered, with 2- and 4-electron reduction pathways. This supports the view that the rate-determining step is influenced by similar factors on the different materials. It has been shown experimentally that there is a relationship between the equilibrium coverage of oxygen at a metal surface (measured in 1 M H_2SO_4 at open circuit with 1 atm of oxygen) and the number of unpaired d-electrons per atom.[64] Also, the heat of adsorption of oxygen has been correlated with the position of the center of the d-band (though there was considerable scatter due to the influence of surface structure).[65]

One interesting aspect of the oxygen reduction system is that the experimental enthalpies of activation do not show

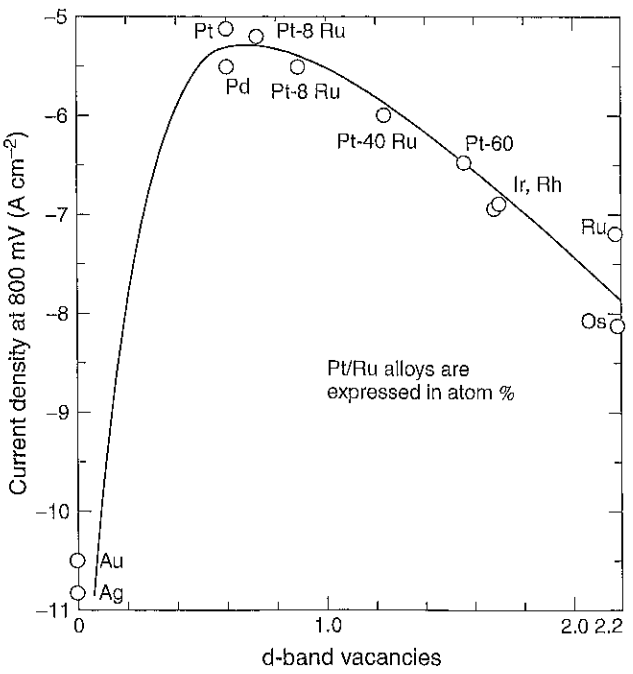

Figure 18. A volcano plot for oxygen reduction versus d-orbital vacancies. (The d-orbital vacancy for Os is considered to be the same as that for Ru). (85% H_3PO_4 and 25 °C; 900 mV vs. RHE corresponds to $\eta = -360$ mV). (Reproduced from Mukerjee *et al.* (1995)[70] by permission of Marcel Dekker, Inc.)

a minimum. Instead, as the metal oxygen bond strength increases, the enthalpy of activation steadily decreases. Examination of the data shows that the steadily decreasing enthalpies of activation are compensated for by a steady decrease in the pre-exponential factor in the rate equation. It is the counterbalancing of these two effects that produces the observed volcano relationships.

As suggested by Appleby,[5, 66] the primary explanation is most likely that, with increasing strength of the metal oxygen bond, a larger fraction of the electrode's surface is covered with adsorbed oxygen species from its equilibrium with water. This results in fewer bare metal sites for the oxygen reduction and so a decrease in the pre-exponential factor of the rate equation. (One interesting reported observation is, for the metals on the Os to Pt side of the volcano, the reaction rates are roughly equal at the potentials at which the adsorbed oxygen layer is reduced.) Thus a catalytic material must balance a strong adsorption of oxygen, to lower the activation enthalpy of the rate-determining step, with a weak adsorption of the oxygen species produced from the reduction reaction and from the equilibrium with water, to have a high coverage of bare metal reaction sites. Among the elements, platinum has the optimum balance of these factors.

To improve the activity of platinum, significant interest has focused on platinum alloys. Platinum has been alloyed with a variety of elements including V, Cr, Si, Ti, Mn, Fe, Co, and Ni. The degree of enhancement of activity obtained with these alloys, and the possible reasons for the observed results, has been an area of much discussion. From a fundamental point of view, important influences of the alloying elements include the inter-atomic spacing and increases in the Pt 5d-orbital vacancies, as well as a possible direct role of surface atoms of the alloying element. This direct role has been suggested to be through interactions with oxygen species or through activity as a redox mediator. Further questions arise because much of this work has been done with dispersed catalyst powders on carbon substrates, and so other factors including variations in particle size may also affect the results. Particle size can affect the specific surface area, and the distribution of atoms between various crystal faces, edge, and corner sites.[67] Another issue is the possible formation of high roughness surfaces, from the selective leaching of the alloying element.

Earlier work focused on phosphoric acid fuel cell conditions (100% H_3PO_4 and 200 °C) and reported enhanced activity due to alloying that could be correlated with the inter-atomic spacing of the catalyst powder as measured by X-ray analysis.[68] Other workers, however, using bulk alloys, noted corrosion of the alloying element leading to surface roughening, which appeared to explain the enhancement.[69] More recent work has shown

that as the inter-atomic spacing decreased, the d-orbital vacancies increased and so the different factors appear to be interrelated (Cr, Mn, Fe, Co, and Ni alloyed with 75 at% Pt, and average catalyst particle sizes from 35 to 69 Å).[70] A volcano type relationship was obtained with an optimum performance for the Pt/Cr alloy, as measured in a proton exchange membrane fuel cell (PEMFC) at 95 °C (see Figure 19). It also appeared that the formation of PtOH was inhibited on the alloys. This led to the suggestion that these alloys allow optimization of the electronic and geometric properties of the catalyst surface, resulting in an increased adsorption of O_2, but also a suppression of reaction site blocking by PtOH formation. This work also observed no change in the oxidation state of the alloying elements in the potential range of oxygen reduction and hence no sign of redox mediation.

The possible role of atoms of the alloying elements at surface sites is controversial. This is because most of the alloying elements would be expected to be most stable as their oxide or hydroxide under normal operating conditions and so might not be expected to be very active.[69, 71] Thus it is felt (and supported by X-ray photoelectron spectroscopy (XPS) surface analysis)[69] that the surface is depleted of alloying elements. Recent work with sputter deposited alloys appears to confirm this view, but suggests that the surface platinum layer is affected by the alloying elements in the sub-surface metal.[72]

Thus, while platinum remains the best catalyst in terms of activity and stability, there appears to be some possibility of fine-tuning its performance.

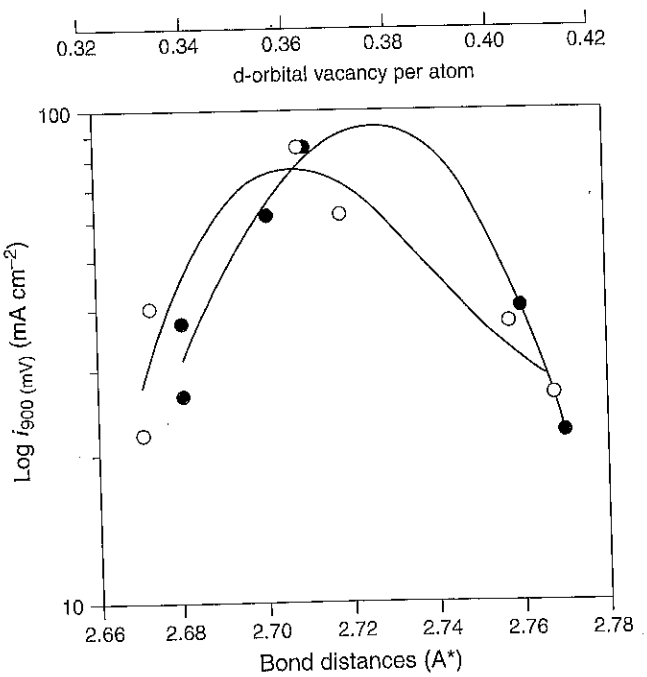

Figure 19. Platinum alloy catalyst performance plotted as a function of measured physical properties. • Pt–Pt bond distance, and ○ d-orbital vacancy of Pt. (Catalyst performance measured in a PEMFC at 95 °C and 5 atm at 900 mV vs. RHE. The physical properties were measured from in situ X-ray adsorption spectroscopy (XAS) in 1 M $HClO_4$). (Reproduced from Mukerjee *et al.* (1995)[70] by permission of The Electrochemical Society.)

6 OXYGEN EVOLUTION

As already discussed, oxygen evolution differs from oxygen reduction in that it takes place on a phase oxide, rather than bare metal. Thus the mechanisms and characteristics of a good catalyst will be different. This is of particular interest for regenerative fuel cells where one type of electrode catalyst system will have to perform both for oxygen evolution and oxygen reduction.

The field of oxygen evolution has been reviewed by Kinoshita.[7] As well as being catalytic, the metal oxide should be stable and conductive. An important concept in oxygen evolution catalysis is the role of the changing valence state of the metal ion. During the discharge of water to form oxygen, various oxygen intermediate species are created (i.e., the reverse of Figure 2). The activation energy to form these intermediates, and their chemical potentials, can be lowered by interaction with the metal atoms in the oxide. This interaction is strong, leading to catalysis, if the metal atom can readily change valence state to form a bond with the intermediate.

This transition of the metal cation in the oxide to a higher valent state (and a higher coordination number) can be written for the first step of water electrolysis (i.e., in acid) as

$$\text{—M—OH} + H_2O \longrightarrow \text{—M(OH)(OH)} + H^+ + e^- \qquad (38)$$

The subsequent steps are often considered to be

$$2MOH \longrightarrow MO + M + H_2O \qquad (39)$$

or possibly

$$MOH \longrightarrow MO + H^+ + e^- \qquad (40)$$

followed by:

$$2MO \longrightarrow 2M + O_2 \qquad (41)$$

In addition, other alternatives may be possible, as can be imagined from the possible intermediates in Figure 2 with the additional inclusion of interactions with the metal

oxide. Thus the mechanism might change with electrode material and also with the cation site geometry. The geometry can change not only the adsorption energy for the oxygen species, but also the activation energy for the change of the cation oxidation state and the related change of its coordination number (e.g., metal cations at edge and defect sites can more easily change their coordination number). This sensitivity to the oxide characteristics can be seen in different activities (exchange current densities and, more significantly, Tafel slopes) for anodes of the same material prepared at different thermal decomposition temperatures.[73] The oxide preparation temperature (and time) can affect characteristics such as the oxide crystallite size, the surface area, the oxide non-stoichiometry (and hence crystal defect sites), and the amount of trapped residual precursor material (often chloride).

For this type of mechanism, it is postulated that catalytic ability should be related to the enthalpy of transition of the oxide from a lower to a higher oxidation state. Metal oxides with a high transition enthalpy will not easily stabilize intermediates. Those with a very low transition enthalpy will form stable higher oxides and so later release of the oxygen species to form O_2 will be slow.[73] This concept can be used to create a volcano plot as shown in Figure 20.

The plot shows reasonable trends, though these should be taken with caution because the plotted values are only approximate. The values are based on averages from a number of sources and proper surface area normalization for many of the materials is difficult. Also, the different materials have different Tafel slopes (and so the plot is possibly not for constant mechanism), and no allowance was made for potential drops caused by the effect of space charge behavior of the polarized oxide films. Others have made a link between the potential for the onset of significant oxygen evolution and the redox potential of the metal cation.[74]

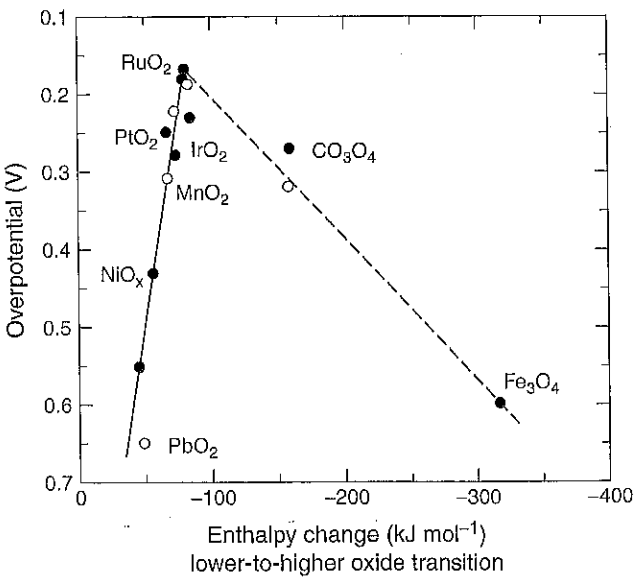

Figure 20. Volcano plot of the overpotential for oxygen evolution versus the enthalpy of the lower to higher oxide transition. ○ Alkaline, and ● acidic solutions. (Reproduced from Trasatti (1984)[73] by permission of Elsevier Science.)

The presence of metal redox couples at the electrode surface is supported by electrode capacitance data as a function of potential. These results for Ni, Co, and Pt show capacitance changes with potential that are consistent, for each metal, with the oxidation of metal cations to a higher valence. As well, this potential corresponds to changes in the Tafel slope for oxygen evolution.[75] An interesting observation was that the slope of potential relaxation curves varied with the starting potential, indicating a possible reconstruction of the electrode surface layer at potentials with a large coverage of higher oxidation state metal cations.

Although platinum and its alloys are the best catalysts for oxygen reduction, they are not the most active materials for oxygen evolution. This is believed to be due to the insulating nature of the platinum oxide film. This film, estimated to be around 10–15 Å thick (depending on the electrode potential and time at that potential), decreases the probability of electron tunneling, which decreases the exchange current density for the reaction.[76] (A slight increase in the symmetry factor, equivalent to a Tafel slope change of about 9 mV decade^{-1} might also be expected.)

The very high activity of RuO_2 and IrO_2-based electrodes for oxygen evolution can therefore be understood because of their relatively low redox potentials (ca. 1.39 and 1.35 V vs. RHE respectively)[74] and the high conductivity of their oxide films. Thus for regenerative PEM fuels cells, a mixed platinum and iridium catalyst (IrO_2 being more stable than RuO_2) is often considered in order to obtain balanced performance for both reactions.[59] Recent work has used a combinatorial approach to optimize catalyst mixtures for PEM regenerative fuel cell applications.[77] After testing 715 combinations of the elements Pt, Ru, Os, Ir, and Rh (prepared by borohydride reduction of the aqueous metal salts) the optimum overall performance was found for $Pt_{4.5}Ru_4Ir_{0.5}$. Combined oxygen evolution and oxygen reduction data are shown in Figure 21. It can be clearly seen that the addition of other metals significantly improves the activity for oxygen evolution versus that for platinum alone, while platinum remains among the best catalysts for oxygen reduction.

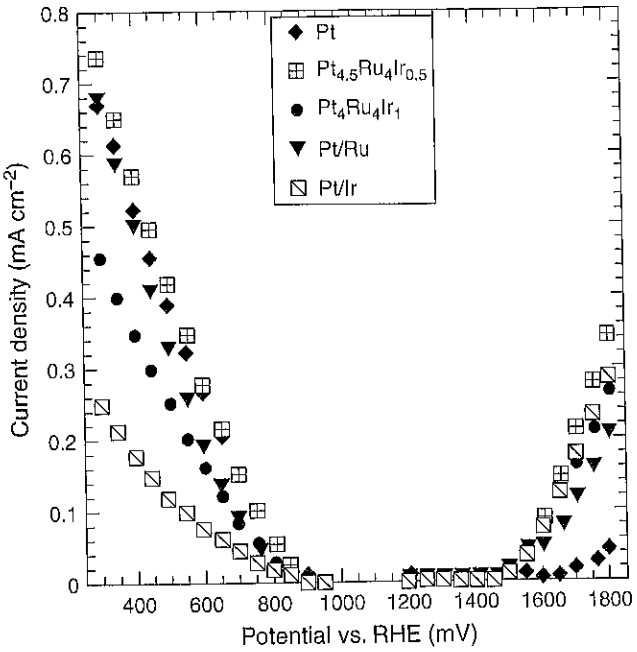

Figure 21. Combined polarization curves of various catalysts for both oxygen evolution and oxygen reduction. (Reproduced from Chen *et al.* (2001)[77] by permission of Elsevier Science.)

7 CONCLUSIONS

The reduction and evolution of oxygen represent important multistep electrocatalytic reactions. Since the early work in this area, our understanding of the complex catalytic interactions between the reactants, the electrode surface, and other adsorbed species has grown greatly. Through new work, this understanding continues to grow in detail and to be expanded to a wider variety of materials and conditions. The following chapters will look at a range of these areas. The study of the oxygen reduction reaction at single crystal surfaces and macrocycle complexes will be covered. The important effects of catalyst particle size and of catalyst particle interactions with its surrounding environment in a fuel cell will be considered. And the reaction in alkaline electrolytes and the wide variety of electrode materials possible under those conditions will be presented. Also, the very different chemistry in molten carbonate and solid oxide fuel cells will be examined.

REFERENCES

1. J. P. Hoare, 'The Electrochemistry of Oxygen', Interscience, New York (1968).
2. A. Damjanovic, 'Mechanistic Analysis of Oxygen Electrode Reactions', in "Modern Aspects of Electrochemistry, No. 5", B. E. Conway and J. O'M. Bockris (Eds), Plenum Press, New York, Ch. 5, pp. 369–483 (1969).
3. J. P. Hoare, 'Oxygen', in "The Encyclopedia of the Electrochemistry of the Elements", A. J. Bard (Ed), Dekker, New York, Vol. 2, pp. 208 (1974).
4. M. R. Tarasevich, A. Sadkowski and E. Yeager, 'Oxygen Electrochemistry' in "Comprehensive Treatise of Electrochemistry", B. E. Conway, J. O'M. Bockris, E. Yeager, S. U. M. Khan and R. E. White (Eds), Plenum Press, New York, Vol. 7, pp. 301–398 (1983).
5. A. J. Appleby, *J. Electroanal. Chem.*, **357**, 117 (1993).
6. A. Damjanovic, 'Progress in the Studies of Oxygen Reduction during the last Thirty Years', in "Electrochemistry in Transition", O. J. Murphy, S. Srinivasan and B. E. Conway (Eds), Plenum Press, New York, pp. 107–126 (1992).
7. K. Kinoshita, 'Electrochemical Oxygen Technology', John Wiley & Sons, New York, pp. 19–65, 99–112 (1992).
8. J. O'M. Bockris and S. U. M. Khan, 'Surface Electrochemistry, A Molecular Level Approach', Plenum Press, New York, pp. 319–49, 394–405 (1993).
9. R. Adzic, 'Recent Advances in the Kinetics of Oxygen Reduction', in "Electrocatalysis", J. Lipkowski and P. N. Ross (Eds), Wiley-VCH, New York, pp. 197–242 (1998).
10. T. E. Springer, M. S. Wilson and S. Gottesfeld, *J. Electrochem. Soc.*, **140**(12), 3513 (1993).
11. M. Pourbaix, 'Atlas of Electrochemical Equilibria in Aqueous Solutions', 2nd Edition, NACE, Houston, pp. 97–105 (1974).
12. A. J. Appleby and F. R. Foulkes, 'Fuel Cell Handbook', Van Nostrand Reinhold, New York (1989).
13. P. C. Foller and R. T. Bombard, *J. Appl. Electrochem.*, **25**, 613 (1995).
14. H. Angerstein-Kozlowska, B. E. Conway and W. B. A. Sharp, *J. Electroanal. Chem.*, **43**, 9 (1973).
15. A. Damjanovic and J. O'M. Bockris, *Electrochim. Acta*, **11**, 376 (1966).
16. D. B. Sepa, M. V. Vojnovic and A. Damjanovic, *Electrochim. Acta*, **26**(6), 781 (1981).
17. A. Damjanovic and V. Brusic, *Electrochim. Acta*, **12**, 615 (1967).
18. D. B. Sepa, M. V. Vojnovic, L. M. Vracar and A. Damjanovic, *Electrochim. Acta*, **32**(1), 129 (1987).
19. M. R. Tarasevich, *Elektrokhimiya*, **9**(5), 599 (1973).
20. D. B. Sepa, M. V. Vojnovic and A. Damjanovic, *Electrochim. Acta*, **26**, 781 (1981).
21. A. N. Fumkin, L. N. Nekrasov, V. G. Levich and Y. B. Ivanov, *J. Electroanal. Chem.*, **1**, 84 (1959).
22. L. Mueller and L. Nekrasov, *Electrochim. Acta*, **9**, 1015 (1964).
23. A. Damjanovic, M. A. Genshaw and J. O'M. Bockris, *J. Electrochem. Soc.*, **114**(5), 466 (1967).
24. A. Damjanovic, M. A. Genshaw and J. O'M. Bockris, *J. Chem. Phys.*, **45**, 4057 (1966).

25. V. S. Bagotskii, M. R. Tarasevich and V. Yu. Filinovskii, *Elektrokhimiya*, **8**(1), 84 (1972).
26. K. L. Hsueh, D. T. Chin and S. Srinivasan, *J. Electroanal. Chem.*, **153**, 79 (1983).
27. H. S. Wroblowa, Y. C. Pan and G. Razumney, *J. Electroanal. Chem.*, **69**, 195 (1976).
28. J. C. Huang, R. K. Sen and E. Yeager, *J. Electrochem. Soc.*, **126**(5), 786 (1979).
29. N. A. Anastasijevic, V. Vesovic and R. R. Adzic, *J. Electroanal. Chem.*, **229**, 305 and 317 (1987).
30. V. S. Vilinskaya and M. R. Tarasevich, *Elektrokhimiya*, **9**(8), 1187 (1973).
31. N. M. Markovic and P. N. Ross, 'Electrocatalysis at Well-Defined Surfaces', in "Interfacial Electrochemistry", A Wieckowski (Ed), Marcel Dekker, New York, pp. 821–841 (1999).
32. C. Puglia, A. Nilsson, B. Hernnais, O. Karis, P. Bennich and N. Martensson, *Surf. Sci.*, **342**, 119 (1995).
33. T. Zambelli, J. V. Barth, J. Wintterlin and G. Ertl, *Nature*, **390**(4), 495 (1997).
34. A. Eichler, F. Mittendorfer and J. Hafner, *Phys. Rev. B*, **62**(7), 4744 (2000).
35. J. L. Gland, B. A. Sexton and G. B. Fisher, *Surf. Sci.*, **95**, 587 (1980).
36. A. B. Anderson and T. V. Albu, *J. Electrochem. Soc.*, **147**(11), 4229 (2000).
37. A. Damjanovic, D. B. Sepa, L. M. Vracar and M. V. Vojnovic, *Ber. Bunsenges. Phys. Chem.*, **90**, 1231 (1986).
38. B. E. Conway, D. F. Tessier and D. P. Wilkinson, *J. Electroanal. Chem.*, **199**, 249 (1986).
39. A. Damjanovic, *J. Electroanal. Chem.*, **355**, 57 (1993).
40. S. J. Clouser, J. C. Huang and E. Yeager, *J. Appl. Electrochem.*, **23**, 597 (1993).
41. E. Gileadi, *J. Electrochem. Soc.*, **134**(1), 117, (1987), and, *J. Electrochem. Soc.*, **137**(12), 3870, (1990).
42. A. J. Appleby, *J. Electroanal. Chem.*, **27**, 325, 335 and 347 (1970).
43. E. Kirowa-Eisner, M. Rosenblum, M. Schwarz, E. Gileadi, *J. Electroanal. Chem.*, **410**, 189 (1996). (And others in the series.)
44. R. R. Adzic, in 'Structural Effects in Electrocatalysis and Oxygen Electrochemistry', D. Scherson, D. Tryk, M. Daroux and X. Xing (Eds), Proceedings of the Electrochemical Society, Pennington, NJ, Vol. 92–11, p. 419 (1992).
45. L. B. Kriksunov, *Electrochim. Acta*, **40**(15), 2553 (1995).
46. B. E. Conway, 'The Temperature and Potential Dependence of Electrochemical Reaction rates, and the Real Form of the Tafel Equation', in "Modern Aspects of Electrochemistry", B. E. Conway, J. O'M. Bockris and R. White (Eds), Plenum, New York, Vol. 16, Ch. 2, pp. 103–188 (1986).
47. J. O'M Bockris and A. Gochev, *J. Phys. Chem.*, **90**, 5232 (1986).
48. E. Yeager, *J. Mol. Catal.*, **38**, 5 (1986).
49. D. B. Sepa, M. V. Vojnovic, L. M. Vracar and A. Damjanovic, *Electrochim. Acta*, **31**(1), 91 and 97 (1986).
50. R. R. Adzic, S. Strbac and N. Anastasijevic, *Mater. Chem. Phys.*, **22**, 349 (1989).
51. R. W. Zurilla, R. K. Sen and E. Yeager, *J. Electrochem. Soc.*, **125**(7), 1103 (1978).
52. R. R. Adzic, N. M. Markovic and V. Vesovic, *J. Electroanal. Chem.*, **165**, 105 and 121 (1987).
53. S. Strbac and R. R. Adzic, *J. Electroanal. Chem.*, **403**, 169 (1996).
54. J. Brooker, P. A. Christensen, A. Hamnett, R. He and C. A. Paliteiro, *Faraday Discuss.*, **94**, 339 (1992).
55. A. J. Appleby and J. Marie, *Electrochim. Acta*, **24**, 195 (1979).
56. J. Xu, W. Huang and R. L. McCreery, *J. Electroanal. Chem.*, **410**, 235 (1996).
57. R. J. Taylor and A. A. Humffray, *J. Electroanal. Chem.*, **64**, 63 (1975).
58. R. L. McCreery, 'Carbon Electrodes: Structural Effects on Electron Transfer Kinetics', in "Electroanalytical Chemistry", A. J. Bard (Ed), Vol. 17, pp. 221–374 (1991).
59. T. Ioroi, N. Kitazawa, K. Yasuda, Y. Yamamoto and H. Takenaka, *J. Appl. Electrochem.*, **31**, 1179 (2001).
60. A. Daghetti, G. Lodi and S. Trasatti, *Mater. Chem. Phys.*, **8**, 1 (1983).
61. D. B. Sepa, M. V. Vojnovic, M. Stojanovic and A. Damjanovic, *J. Electroanal. Chem.*, **218**, 265 (1987).
62. D. B. Sepa, M. V. Vojnovic, M. Stojanovic and A. Damjanovic, *J. Electrochem. Soc.*, **134**(4), 845 (1987).
63. A. A. Balandin, 'Problems of Chemical Kinetics, Catalysis and Reactivity', Academy of Sciences, Moscow, pp. 462, (1955).
64. M. L. B. Rao, A. Damjanovic, J. O'M. Bockris, *J. Phys. Chem.*, **67**, 2508 (1963).
65. C. Lu, I. C. Lee, R. I. Masel, A. Wieckowski and C. Rice, *J. Phys. Chem. A*, **106**, 3084 (2002).
66. A. J. Appleby, 'Electrocatalysis' in "Comprehensive Treatise of Electrochemistry", B. E. Conway, J. O'M Bockris, E. Yeager, S. U. M. Khan and R. E. White (Eds), Plenum Press, New York, Vol. 7, pp. 173–239 (1983).
67. A. J. Appleby, *Catal. Rev.*, **4**, 221 (1970).
68. V. Jalan and E. J. Taylor, in 'The Chemistry and Physics of Electrocatalysis', J. D. E. MacIntyre, M. J. Weaver and E. B. Yeager (Eds), Proceedings of the Electrochemical Society, Pennington, NJ, Vol. 84–12, p. 546 (1984).
69. M. T. Paffett, J. G. Beery and S. Gottesfeld, *J. Electrochem. Soc.*, **135**(6), 1431 (1988).
70. S. Mukerjee, S. Srinivasan, M. P. Soriaga and J. McBreen, *J. Electrochem. Soc.*, **142**(5), 1409 (1995).
71. A. B. Anderson, E. Grantscharova and S. Seong, in 'Oxygen Electrochemistry', R. R. Adzic, F. C. Anson and K. Kinoshita (Eds), Proceedings of the Electrochemical Society, Pennington, NJ, Vol. 95–26, p. 1 (1996).
72. T. Toda, H. Igarashi and M. Watanabe, *J. Electrochem. Soc.*, **146**(10), 3750 (1999).
73. S. Trasatti, *Electrochim. Acta*, **29**(11), 1503 (1984).

74. P. Rasiyah and A. C. C. Tseung, *J. Electrochem. Soc.*, **131**(4), 803 (1984).

75. B. E. Conway and T. C. Liu, *Mat. Chem. Phys.*, **22**, 163 (1989).

76. A. Damjanovic, V. I. Birss and D. S. Boudreaux, *J. Electrochem. Soc.*, **138**(9) 2549 (1991).

77. G. Chen, D. A. Delafuente, S. Sarangapani and T. E. Mallouk, *Catal. Today*, **67**, 341 (2001).

Handbook of Fuel Cells

Fundamentals Technology and Applications

VOLUME 2
Electrocatalysis

Editors

Wolf Vielstich
IQSC, São Carlos, Universidade de São Paulo, Brazil

Arnold Lamm
DaimlerChrysler Research and Technology, Ulm, Germany

Hubert A. Gasteiger
Fuel Cell Activities, General Motors Corporation, Honeoye Falls, NY, USA

WILEY

The Atrium,
Southern Gate,
Chichester,
West Sussex
PO19 8SQ, England

Telephone (+44) 1243 779777

Email (for orders and customer service enquiries): cs-books@wiley.co.uk
Visit our Home Page on www.wileyeurope.com or www.wiley.com

Cover Images

Foreground: Double height Ru islands grown on Pt(III) at 400 K. Reproduced from H. Hoster *et al*, *Physical Chemistry Chemical Physics*, **3**, 337–346 (2001) by permission of the Royal Society of Chemistry on behalf of the PCCP Owner Societies.
Background: Figure showing MSVC of Ethanol at Porous Platinum in H_2SO_4. Reproduced from T. Iwasita, *J Braz Chem Soc*, **13**, 401–409 (2002), by permission of Sociedade Brasileira de Quimica [Brazilian Chemical Society].

Other Wiley Editorial Offices

John Wiley & Sons Inc., 111 River Street,
Hoboken, NJ 07030, USA

Jossey-Bass, 989 Market Street,
San Francisco, CA 94103-1741, USA

Wiley-VCH Verlag GmbH, Boschstr. 12,
D-69469 Weinheim, Germany

John Wiley & Sons Australia Ltd, 33 Park Road,
Milton, Queensland 4064, Australia

John Wiley & Sons (Asia) Pte Ltd, 2 Clementi Loop #02-01,
Jin Xing Distripark, Singapore 129809

John Wiley & Sons Canada Ltd, 22 Worcester Road,
Etobicoke, Ontario, Canada M9W 1L1

Wiley also publishes its books in a variety of electronic formats. Some content that appears in print may not be available in electronic books.

British Library Cataloguing in Publication Data

A catalogue record for this book is available from the British Library

ISBN: 0-471-49926-9

Typeset in 10/12.5pt Times by Laserwords Private Limited, Chennai, India
Printed and bound in Italy by Rotolito Lombardo, Milan, Italy.
This book is printed on acid-free paper responsibly manufactured from sustainable forestry in which at least two trees are planted for each one used for paper production.